CHAPTER

FOUR

THE ZONAL METHOD: A PRACTICAL SOLUTION METHOD FOR RADIATIVE TRANSFER IN NONISOTHERMAL INHOMOGENEOUS MEDIA

Walter W. Yuen and Ezra E. Takara

ABSTRACT

This is a comprehensive review of the zonal method. In addition to presenting the fundamentals of the method, sufficient details and numerical data are included so that this work can serve as a "user guide" of the method for practical applications. A review of the mathematical properties of the exchange factor indicates that the traditional "diffusion approximation" of radiative heat flux when expressed in finite difference form is in error even in the optically thick limit. Illustrative examples are presented to show the capability of the zonal method in simulating radiative heat transfer in inhomogeneous, nonisothermal media, including the effect of opaque obstructions. The method is extented to become the generalized zonal method (GZM) for applications in anisotropically scattering media. Numerical examples with small number of grid points are presented to demonstrate the capability of the method. With advances in parallel computing and large memory data storage and retrieval, GZM has excellent potential of becoming a practical approach for the analysis of radiative heat transfer in practical engineering systems.

NOMENCLATURE

a	absorption coefficient
A	area

$\bar{A}$	effective bandwidth
B	wide band correlation parameter, Eq. (34)
C	wide band correlation parameter, Eq. (33)
C_1	wide band correlation parameter, Eq. (33)
C_3	wide band correlation parameter, Eq. (33)
d	wide band correlation parameter, Eq. (35)
D	dimension of cube-square system
E_b	blackbody emissive power
f_v	volume fraction
F_{gg}	normalized volume-volume exchange factor
$F_{gg,t}$	sum of normalized volume-volume exchange factor
F_{gs}	normalized volume-area exchange factor
F_{ssp}	normalized exchange factor between parallel square areas
F_{sst}	normalized exchange factor between perpendicular square areas
g_ig_j	exchange factor between V_i and V_j
g_is_j	exchange factor between V_i and A_j
H	irradiation
k	extinction coefficient, also complex index of refraction
L_{ab}	absorption mean beam length
M	number of volume elements in an enclosure
n	real index of refraction
N	number of area elements in an enclosure, also particle number density
$\vec{n}$	normal unit vector
P_A	pressure of absorbing gas, Eq. (36)
P_B	pressure of broadening gas, Eq. (36)
P_e	effective pressure, Eq. (36)
q	heat flux
Q	heat transfer
Q_{abs}	absorption cross section, Eq. (37)
Q_{ext}	extinction cross section, Eq. (37)
r	radial distance, Eq. (2), also particle radius
$\vec{r}$	radial vector
R	radial distance parameter
R_o	radius of furnace, Figure 18
s	distance, Eq. (4)
s_is_j	exchange factor between A_i and A_j
s_ig_j	exchange factor between A_i and V_j
S	heat generation
T	temperature
V	volume
W	radiosity
x	coordinate
X	distance parameter
y	coordinate

Y	distance parameter
z	coordinate
Z	distance parameter

Greek

ε	emissivity, also emittance
η	dimensionless distance coordinate
θ	angular variable
λ	wavelength
ν^*	wavenumber
ϕ	angular variable
Φ	phase function
$\hat{\Phi}$	average phase function
ρ''	bidirectional reflectivity
ρ	density
$\hat{\rho}$	average reflectivity
τ	optical thickness, Eq. (3), also transmittance
ω	scattering albedo

Subscript

0	reference value
a	average
g	gas
i	index for volume (area)
j	index for volume (area)
m	medium
p	particle
t	total
tot	total
w	wall

1 INTRODUCTION

In the analysis of high-temperature engineering systems such as industrial furnaces, the need for an efficient and accurate solution method for radiative heat transfer in participating media is well known. However, after much effort over the last 50 years, the issue of developing such a solution method for radiation heat transfer is still not completely resolved. For the practicing engineer, the quantification of the effect of radiation heat transfer in "real" engineering system within an acceptable degree of accuracy is still considered a difficult task.

In general, the existing solution methods for radiative heat transfer can be classified into two groups, each with its own difficulties and limitations. First, there is a group of solution methods that consider radiative transfer as a diffusion process (e.g., the various differential methods and their modification, P-N method and multi-flux methods). Although these methods have the advantage of computational simplicity, their accuracy is highly uncertain because the formulation is inaccurate both in the optically thin and thick limit. In an optically thin system, radiative transfer strongly depends on geometry and cannot be simulated as a diffusion process. As shown in Section 2, the traditional "diffusion" formulation of the radiative heat flux is incorrect, even in the optically thick limit. The second group of solution methods model radiative heat transfer by simulating "exactly" the geometrical effect of photon transport. The discrete-ordinate method, the Monte Carlo method, and their modifications are examples of such an approach. However, whereas these methods are effective in simulating radiative transfer in the optically thin limit, they are time consuming (even by standard of modern supercomputers) and impractical for applications in "real" engineering calculations. It should be noted that because of the highly spectral-dependent and band-like behavior of gaseous absorption, an accurate simulation of radiative transport in a combustion medium requires a solution method that is accurate and computationally efficient over the complete range of optical thickness. Indeed, the lack of such a solution method is probably one of the main obstacles to the implementation of many recent radiation-related research innovations to practical engineering systems (e.g,, soot-laden flame for high emissivity/absorptivity, high emission porous burner, the use of laser in material processing, etc.). For practicing engineers, the estimate of the effect of radiation in "real" system remains "too complicated" and "too imprecise".

The objective of this work is to present a comprehensive review of the zonal method and to show that it is a suitable method for analysis of radiative heat transfer in practical engineering systems. The method, developed by Hottel and co-workers [1–4] over the last 40 years, has not received much attention from the research community because it was originally proposed and generally perceived by many as a method of calculating radiative exchange involving an isothermal gas, not as a method of solution to the equation of radiative transfer. Indeed, in some recent textbooks on radiation heat transfer, the zonal method was either totally ignored [5] or mentioned in the context of "engineering treatment of radiative heat transfer in enclosure" [6] and separated from the discussion of solution methods for the equation of radiative transfer.

Another possible explanation on the lack of attention on the zonal method is the perception that it is computationally intensive, particularly in the evaluation of the required exchange factors. The method is also perceived as not applicable for scattering media and difficult to apply to combined mode problems and/or nongray problems. Whereas some of these perceived difficulties are real and have not been completely resolved, much improvement has been attained in recent years due to advances in computational power and an improved understanding of the mathematics of the zonal method. The present work intends to review such advances and to give

an up-to-date perspective on the capability of the zonal method as a computational tool for radiative heat transfer in practical engineering systems.

The present review and discussion of the zonal method is organized into six separate sections. In Section 2, the definition and the mathematical properties of the zonal exchange factors are reviewed. A set of "generic" normalized exchange factors are shown to be applicable for analysis of three-dimensional radiative heat transfer in inhomogeneous media (note that in this work the term "inhomogeneous media" means media with nonuniform radiative properties). Based on the mathematical behavior of these factors, a concept of "radiation length" is introduced to account for the increasingly "localized" effect of radiative heat transfer in media of finite optical thickness. This concept is shown to be effective in reducing the computational complexity. In the optically thick limit, the traditional diffusion approximate approximation for the radiative heat flux is shown to be inaccurate. In Section 3, equations of energy balance based on the zonal method are presented. A network analogy is shown to exist and the method is demonstrated to be applicable for three-dimensional absorbing, emitting, and isotropically scattering media. Solutions to nongray problems are generated by integration of tabulated gray solutions covering the range of optical properties. This method is shown to be particularly effective if the nongray region is confined to a finite number of localized subvolumes. Combined-mode problems are observed to be most effectively solved by parallel computation. In Section 4, results of some sample calculations are presented to demonstrate the capability of the method. In Section 5, an extension of the zonal method to anisotropically scattering media is discussed. Some approximate results are presented and the computational requirement for a more detailed solution is discussed. Finally, a conclusion to the present review is presented in Section 6.

It is important to note that the present review was written to be more than a description of the "fundamentals" of the zonal method. Sufficient details and numerical data are included so that this work can also serve as a "user guide" to the zonal method for practical applications.

2 THE MATHEMATICS OF EXCHANGE FACTORS

The concept of exchange factors (also called direct-interchange areas) was introduced by Hottel and co-workers [1–4] in their original formulation of the zonal method. In this review, some key concepts and properties of these factors, particularly those that are important for the application of the method in inhomogeneous media, are discussed. These results are the cumulation of contributions from many researchers [1–4,7–11].

2.1 Definition and the Concept of "Generic" Exchange Factor

Physically, the exchange factor between two volume elements, V_i and V_j represents the energy radiated from V_i and "extinguished" (i.e., absorbed and scattered) by V_j. Mathematically, it is written formally as

$$g_i g_j = \int_{V_i}\int_{V_j} \frac{k_i k_j e^{-\tau} dV_i dV_j}{\pi r^2} \tag{1}$$

where

$$r = \left[\left(x_i - x_j\right)^2 + \left(y_i - y_j\right)^2 + \left(z_i - z_j\right)^2\right]^{\frac{1}{2}} \tag{2}$$

and τ is the optical thickness between the differential volume element dV_i and dV_j given by

$$\tau = \int_{\vec{r}_i}^{\vec{r}_j} k(s)ds \tag{3}$$

with

$$s = \left|\vec{r} - \vec{r}_i\right| \tag{4}$$

and the integration is performed along a straight line extending from $\vec{r}_i$ to $\vec{r}_j$.

In a similar manner, the exchange factor between a volume element V_i and an area element A_j, and that between two area elements A_i and A_j are given, respectively, by

$$g_i s_j = \int_{V_i}\int_{A_j} \frac{k_i e^{-\tau}\left|\vec{n}_j \cdot \vec{r}\right| dV_i dA_j}{\pi r^3} \tag{5}$$

$$s_i s_j = \int_{A_i}\int_{A_j} \frac{e^{-\tau}\left|\vec{n}_j \cdot \vec{r}\right|\left|\vec{n}_i \cdot \vec{r}\right| dA_i dA_j}{\pi r^4} \tag{6}$$

where $\vec{n}_i$ and $\vec{n}_j$ are unit normal vectors of area element dA_i and dA_j.

The numerical evaluation of Eqs. (1), (5) and (6) is complex if the integrand has a singular point ($r = 0$). This arises in the exchange factor for a volume zone to itself (self-self exchange factor; $g_i g_i$) and exchange factors between adjacent zones. The proper evaluation of the self-self and adjacent zone exchange factors is necessary to model the radiative transfer to the other zones in the enclosure and thus enable an accurate solution. As the optical thicknesses increase, the self-self and adjacent factors become more important, while computing them becomes more difficult. This is one of the primary difficulties of the zonal method.

Over the last 20 years, the understanding of the analytical behavior of these exchange factors has been improved significantly [7–11]. Together with the increased computational power and storage capacity associated with modern computers, the difficulty associated with the evaluation of exchange factors has been resolved. Specifically, a "generic" set of exchange factors applicable to most practical geometries of interest can be tabulated. For practicing engineers, these tabulated values constitute a convenient and useful set of numerical data based on which the effect of radiative heat transfer can be estimated.

A useful set of "generic" exchange factors are those for a cube-square system in which all volumes are cubes and all areas are squares with both the cube edge and the square side designated as D. As noted by previous investigators [2,11], all enclosures of industrial importance can be adequately approximated as a cube-square system.

For cubical volumes with geometry as shown in Figure 1, and, assuming that the extinction coefficient within a volume zone is constant, Eq. (1) can be reduced into the following normalized form

$$\frac{g_i g_j}{k_i k_j D^4} = F_{gg}\left(k_{a,ij}D, \eta_X, \eta_Y, \eta_Z\right) = \int_0^1\int_0^1\int_0^1\int_0^1\int_0^1\int_0^1 \frac{e^{-k_{a,ij}D\eta_r} d\eta_{x,i} d\eta_{y,i} d\eta_{z,i} d\eta_{x,j} d\eta_{y,j} d\eta_{z,j}}{\pi\eta_r^2} \tag{7}$$

where $k_{a,ij}$ is the average extinction coefficient between V_i and V_j given by

$$k_{a,ij} = \frac{\tau}{r} = \frac{1}{r}\int_{\vec{r}_i}^{\vec{r}_j} \mathrm{k(s)ds} \tag{8}$$

In Eq. (7), η is the normalized distance given by

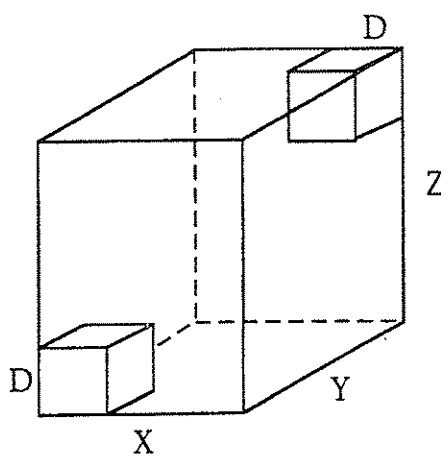

Figure 1 Geometry of the two cubical volumes for the exchange factor $g_i g_j$.

$$\eta_x = \frac{x}{D}, \quad \eta_y = \frac{y}{D}, \quad \eta_z = \frac{z}{D}, \quad \eta_r = \frac{r}{D} \tag{9a}$$

and

$$\eta_X = \frac{X}{D}, \quad \eta_Y = \frac{Y}{D}, \quad \eta_Z = \frac{Z}{D} \tag{9b}$$

Similarly, for geometry as shown in Figure 2, the normalized expression for $g_i s_j$ is

$$\frac{g_i s_j}{k_i D^3} = F_{gs}\left(k_{a,ij} D, \eta_X, \eta_Y, \eta_Z\right) = \int_0^1\int_0^1\int_0^1\int_0^1\int_0^1 \frac{e^{-k_{a,ij} D \eta_r} \left|\eta_{x,i} - \eta_{x,j}\right| d\eta_{x,i} d\eta_{y,i} d\eta_{z,i} d\eta_{x,j} d\eta_{y,j}}{\pi \eta_r^3} \tag{10}$$

In the evaluation of $s_i s_j$, there are two possibilities. For two parallel areas as shown in Figure 3, it is

$$\frac{s_i s_j}{D^2} = F_{ssp}\left(k_{a,ij} D, \eta_X, \eta_Y, \eta_Z\right) = \int_0^1\int_0^1\int_0^1\int_0^1 \frac{e^{-k_{a,ij} D \eta_r} \left|\eta_{z,i} - \eta_{z,j}\right|^2 d\eta_{x,i} d\eta_{y,i} d\eta_{x,j} d\eta_{y,j}}{\pi \eta_r^4} \tag{11}$$

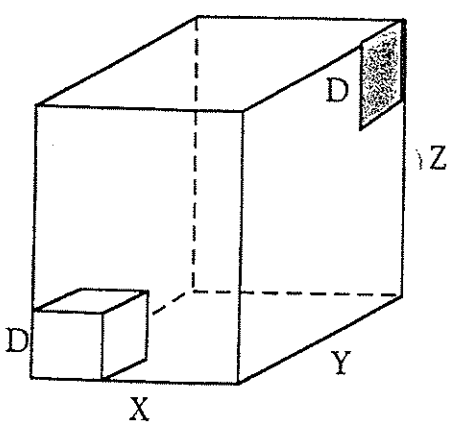

Figure 2 Geometry of the cubical volume and square for the exchange factor $g_i s_j$.

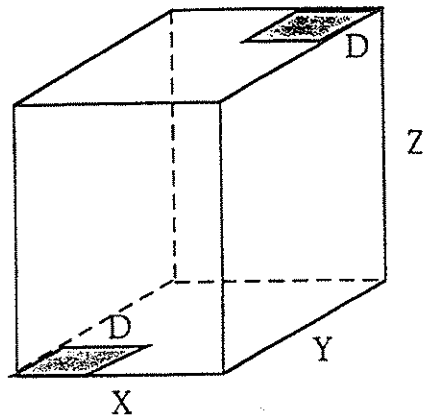

Figure 3 Geometry of the two parallel squares for the exchange factor $s_i s_j$.

and for two perpendicular areas as shown in Figure 4, it is

$$\frac{s_i s_j}{D^2} = F_{sst}\left(k_{a,ij} D, \eta_X, \eta_Y, \eta_Z\right) = \int_0^1\int_0^1\int_0^1\int_0^1 \frac{e^{-k_{a,ij} D \eta_r} \left|\eta_{z,i} - \eta_{z,j}\right| \left|\eta_{x,i} - \eta_{x,j}\right| d\eta_{x,i} d\eta_{y,i} d\eta_{y,j} d\eta_{z,j}}{\pi \eta_r^4} \tag{12}$$

It is important to note that with $k_{a,ij}$ interpreted as the average extinction coefficient as given by Eq. (8) varies among the different lines of sight connecting the two

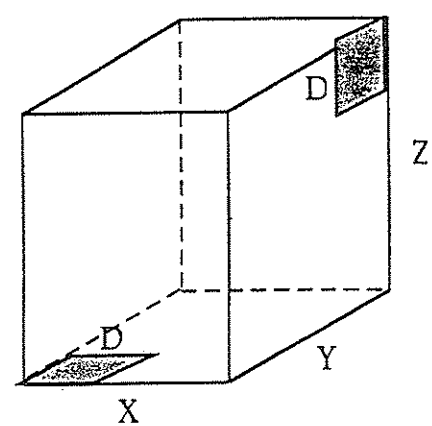

Figure 4 Geometry of the two perpendicular squares for the exchange factor $s_i s_j$.

elements. The evaluation of these normalized factors with $k_{a,ij}$ treated as constant is thus an approximation when D is finite. However, as D $\rightarrow$ 0, the different lines of sight become increasingly "identical" and these factors are "exact". Tabulated values of the four normalized exchange factors for some discrete values of optical thicknesses and geometric factors are presented in Appendix A. A summary of the evaluation procedure is also included for the convenience of additional tabulation, if needed, by the reader.

2.2 Properties of "Generic" Exchange Factor and the Concept of "Radiation Length"

The "generic" exchange factors have some mathematical properties that can lead to important simplification for practical applications. For media with finite optical thickness, these factors can be used to illustrate the degree of localization of the radiative effect. For example, the absorption of emission from a cubical element by its neighboring cubical elements within a distance L can be characterized by the following summation factor

$$F_{gg,t}\left(kD,\frac{L}{D}\right)=\sum_{\eta_R\le\frac{L}{D}} F_{gg}\left(kD,\eta_X,\eta_Y,\eta_Z\right) \tag{13}$$

with

$$\eta_R=\left(\eta_X^2+\eta_Y^2+\eta_Z^2\right)^{\frac{1}{2}} \tag{14}$$

Physically, $F_{gg,t}$ represent the "normalized" fractional extinction by cubical elements within a distance L of the emitting cube. Because the emitted energy must be extinguished by all cubes, $F_{gg,t}$ is expected to have the following limiting behavior

$$\sum_{\frac{L}{D}\rightarrow\infty} F_{gg,t}\left(kD,\frac{L}{D}\right)=\frac{4}{kD} \tag{15}$$

The mathematical behavior of $F_{gg,t}$ as a function of kD and $\frac{L}{D}$ is shown in Figure 5. As kD increases, $F_{gg,t}$ approaches its limiting value quickly. Direct examination of numerical data shows that for $kD \ge 2$, energy conservation can be achieved to within 0.1% by summing exchange factors with $\frac{L}{D} \le 3.75$. Mathematically, these results suggest that in a zonal calculation, direct radiative exchange between two cubical elements can be ignored when $kD \ge 2$ and $\frac{L}{D} > 3.75$, or when the optical distance between the two cubic elements is greater than 7.5.

The above result is consistent with the "radiation length" concept originally proposed by Yuen and Ma [12]. Specifically, based on results of three one-dimensional calculations, it was concluded that the radiative exchange between nonadjacent volume elements can be ignored if the optical distance between them is greater than 7.5. Direct comparison between the exact zonal results and the zonal results generated with the radiation-length concept for two of the three one-dimensional test problems generated in this previous work [12] are shown in Figures 6a and 6b. This concept can be used to reduce the numerical complexity of the zonal calculation. Even though the numerical examples are presented only for homogeneous media, the "radiation-length" concept is expected to be applicable for general inhomogeneous media.

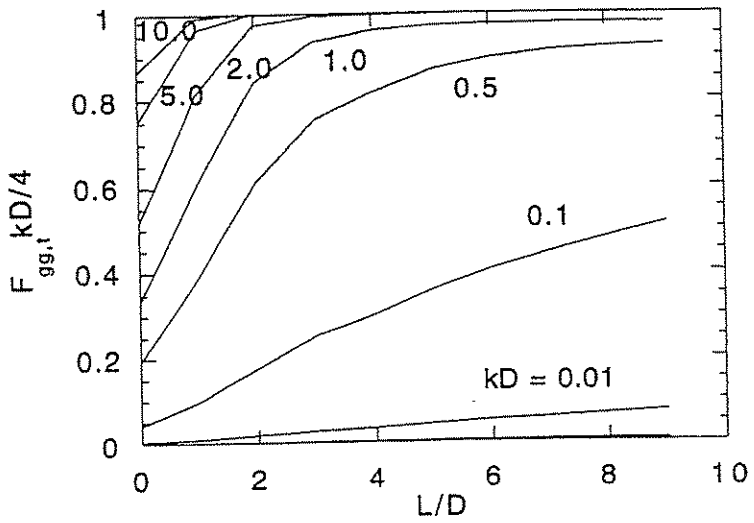

Figure 5 Mathematical behavior of $F_{gg,t}$.

Another important mathematical property of the exchange factor is illustrated by the behavior of the exchange factor between adjacent volume elements. Physically, a finite nonscattering volume element becomes a black body emitter in the optically thick limit. For two adjacent nonscattering finite volume elements of dimension D, the optically thick limit of the radiative heat transfer (assuming that one volume is emitting with emissive power E_b and the second volume is "cold" at zero degree) is thus given by

$$\lim_{kD\rightarrow\infty} Q = E_b D^2 \tag{16}$$

This suggests the following limiting behavior for F_{gg},

$$\lim_{kD\rightarrow\infty} F_{gg}(kD,2,1,1) = \frac{1}{(kD)^2} \tag{17}$$

The accuracy of Eqs. (16) and (17) are confirmed by numerical data presented in Figure 7.

Eqs. (16) and (17) illustrate an important misconception about the diffusion limit of radiative heat transfer. In practically all of the existing literature on radiation heat

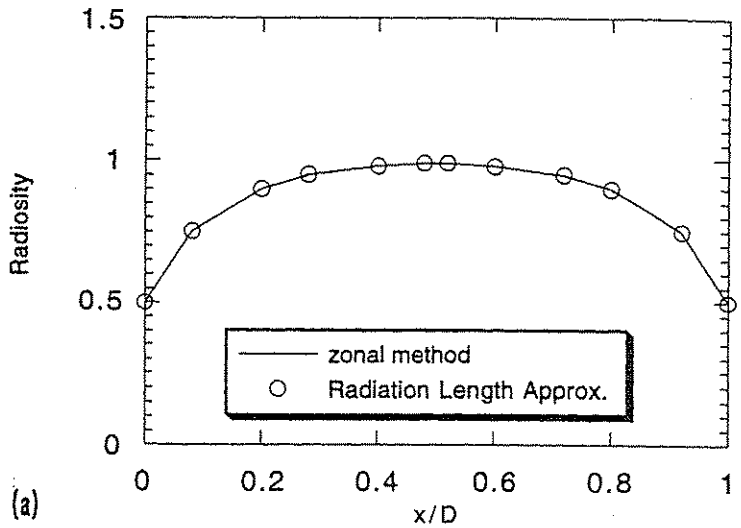

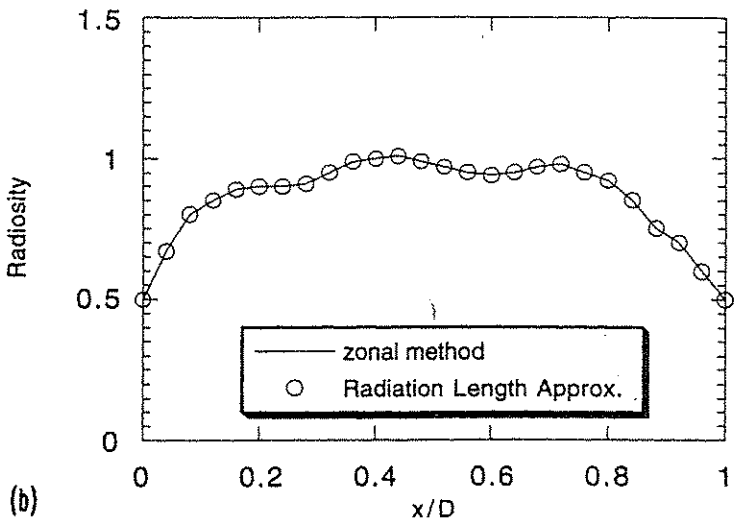

Figure 6a,b (a) Radiosity distribution of a slab of uniform temperature with kD = 10 and ω = 0.8. (b) Radiosity distribution of a slab of isotropically scattering medium with a sinusoidal temperature distribution $E_b(x) = 1 + 0.8sin\left(\frac{5\pi x}{D}\right)$. The optical thickness kD and scattering albedo ω are identical to those of (a).

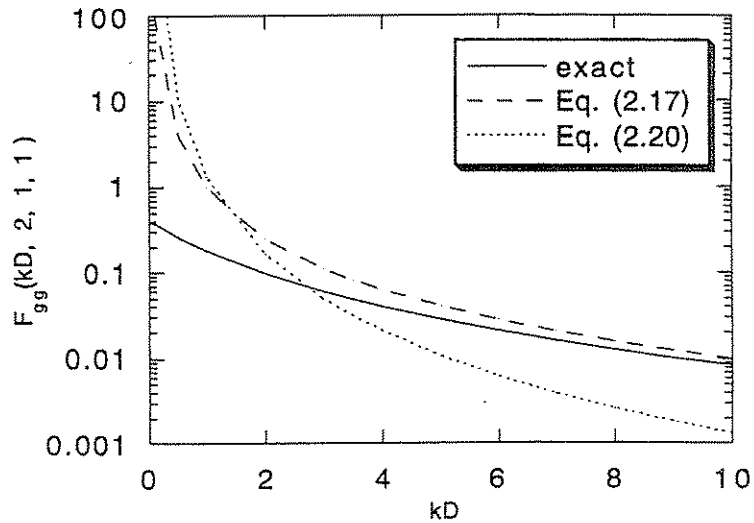

Figure 7 Comparison between $F_{gg}(kD,2,1,1)$ and the two limiting expressions, Eqs. (17) and Eqs. (20).

transfer [5,6], the radiative heat flux (for example, in the x direction) in the diffusion limit is always written as

$$q = -\frac{4}{3k}\frac{dE_b}{dx} \tag{18}$$

and, for numerical application, expressed in the following finite difference form

$$q = -\frac{4}{3k}\frac{E_b(x+\Delta x) - E_b(x)}{\Delta x} \tag{19}$$

Utilizing Eq. (19), the "diffusion" approximation of the normalized exchange factor between two adjacent volume elements becomes

$$\lim_{kD\to\infty} F_{gg,d}(kD,2,1,1) = \frac{4}{3(kD)^3} \tag{20}$$

Eq. (20) is also plotted in Figure 7 for a direct comparison with the exact result.

Eqs. (19) and (20) are clearly in error as they do not approach the correct physical limit as described by Eqs. (16) and (17). The fundamental difficulty can be attributed to the volumetric nature of radiative emission and extinction. Specifically, Eq. (18) is derived for two discrete points in the limit of large optical thickness between these

discrete points. In the evaluation of radiative exchange between adjacent volume elements with finite dimension, on the other hand, the radiative heat transfer is the summation of radiative exchange between many discrete subvolumes within the two volume elements. Because two adjacent volume elements share a common interface, there are always discrete subvolumes for which the diffusion approximation (Eq. (18)) fails even in the limit of $k \to \infty$. In fact, the radiative exchange between subvolumes near the interface (with essentially zero distance between them) dominates the heat transfer in the optically thick limit. The effect is captured by Eq. (16) and not by Eq. (19).

It is interesting to note that despite the inaccuracy, the finite difference equations generated by Eq. (19) for a one-dimensional planar system is identical to those generated by the zonal method in the optically thick limit. This explains the many "agreements" reported in the literature between the diffusion approximation and the "exact" results. Indeed, the need to introduce a temperature slip and to apply a separate heat balance condition at the boundary in the mathematical solution based on the diffusion approximation can be attributed directly to this physical inconsistency. Unfortunately, the diffusion approximation is often used by the practicing engineering community as a "first check" of the radiation effect. This has led to many erroneous underestimates of the effect of radiation heat transfer in practical engineering systems.

2.3 Summary

In summary, the evaluation of exchange factors needed for the zonal method is a "solved" problem because of the improved mathematical understanding and the increased computational power and storage associated with modern computers. A set of "generic" normalized exchange factors for a cube-square system are presented. They are applicable for inhomogeneous media and most practical enclosures of industrial importance.

Two important mathematical properties of the normalized exchange factor are identified. First, a concept of "radiation length" is effective in illustrating the localized nature of radiative transfer in the limit of large optical thickness. Numerically, this length is estimated to be about 7.5. The radiative exchange between disjoint volume elements with optical distance greater than 7.5 can be ignored without affecting the accuracy of the numerical solution. Second, the commonly accepted diffusion approximation of radiative heat flux is shown to be inaccurate even in the optically thick limit. It underpredicts the radiative heat transfer and thus can lead to an erroneous underestimate of the importance of radiative heat transfer in practical engineering systems.

3 MATHEMATICAL FORMULATION

One of the attractive features of the zonal method is the simplicity of the governing equations. For an absorbing, emitting, and isotropically scattering medium, the mathematical formulation is formally equivalent to that associated with the analysis of an electrical network. The basic governing equation is in the form of a matrix equation. The matrix elements are expressed in a systematic repeatable manner that can be easily adapted into a computer program. Because the matrix is "dense", a primary difficulty of the zonal method has been the intense computational effort and large storage requirement associated with the matrix inversion (particularly when the number of volume and surface elements is large). However, with the rapid advance achieved in modern computational technology, this difficulty is becoming less significant and the zonal method can now be considered a practical solution method.

In this section, the electrical network analogy is first presented in Section 3.1 to illustrate the simple physics of radiative exchange and its mathematical symmetry. The formal development of the governing equations is presented in Section 3.2. The methodology for extending the zonal method to nongray problem, together with a discussion of the usage of zonal method in combined mode problem, are presented in Section 3.2. Extension of the method to anisotropically scattering media is deferred until a later section (Section 5).

3.1 The Network Analogy

The physical basis of the network analogy is that for both diffuse surface and isotropically scattering volume elements, the emitted and reflected (or scattered) intensity leaving each element are isotropic. This leads to the concept of "radiosity", W_i and $W_{g,i}$, which are related to the "outgoing" intensity by

$$\frac{W_i}{\pi} = \text{intensity (emission plus reflection) leaving surface } A_i$$

$$\frac{W_{g,i}}{\pi} = \text{intensity (emission plus scattering) leaving volume } V_i$$

These radiosities are responsible for the radiative exchange between volume (area) elements with the appropriate exchange factor playing the role of a "resistance". Because the intensity leaving a surface (or volume) element consists of both the emitted and reflected (or scattered) intensity, the radiosity is a function of the emissive power and the radiative properties as shown in the next subsection.

Schematic representations of the network analogy for a surface element A_i and a volume element V_i are shown in Figures 8 and 9, respectively. Specifically, the analogy between electrical network and radiative heat transfer in an absorbing, emitting, and isotropically scattering medium is

$$E_{b,i} = \text{internal potential of area } A_i$$

$$W_i = \text{external potential of area } A_i$$

$$\frac{1-\varepsilon_i}{A_i\varepsilon_i} = \text{internal resistance of surface } A_i$$

$$E_{bg,i} = \text{internal potential of volume } V_i$$

$W_{g,i}$ = external potential of volume V_i

$\frac{\omega_i}{4k_iV_i(1-\omega_i)}$ = internal resistance of volume V_i

$\frac{1}{s_is_j}$ = resistance between surfaces A_i and A_j

$\frac{1}{s_ig_j}$ = resistance between surface A_i and volume V_j

$\frac{1}{g_ig_j}$ = resistance between volume V_i and V_j

It is important to note that the network analogy does not require the assumption of a homogeneous medium. If the variation of radiative properties between two elements is accounted for in the evaluation of the exchange factor, as discussed in Section 2. The analogy is applicable to any enclosure containing an absorbing, emitting, and isotropically scattering medium.

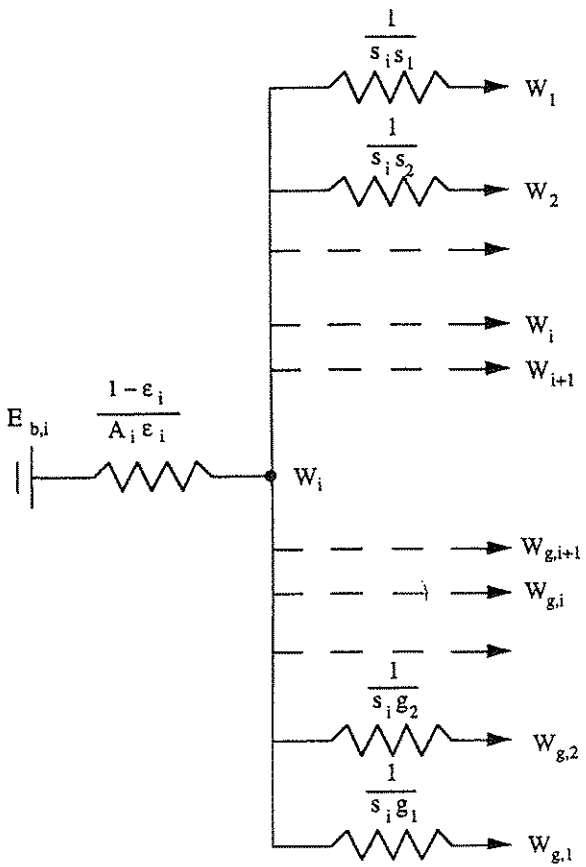

Figure 8 Network representation of a surface element A_i.

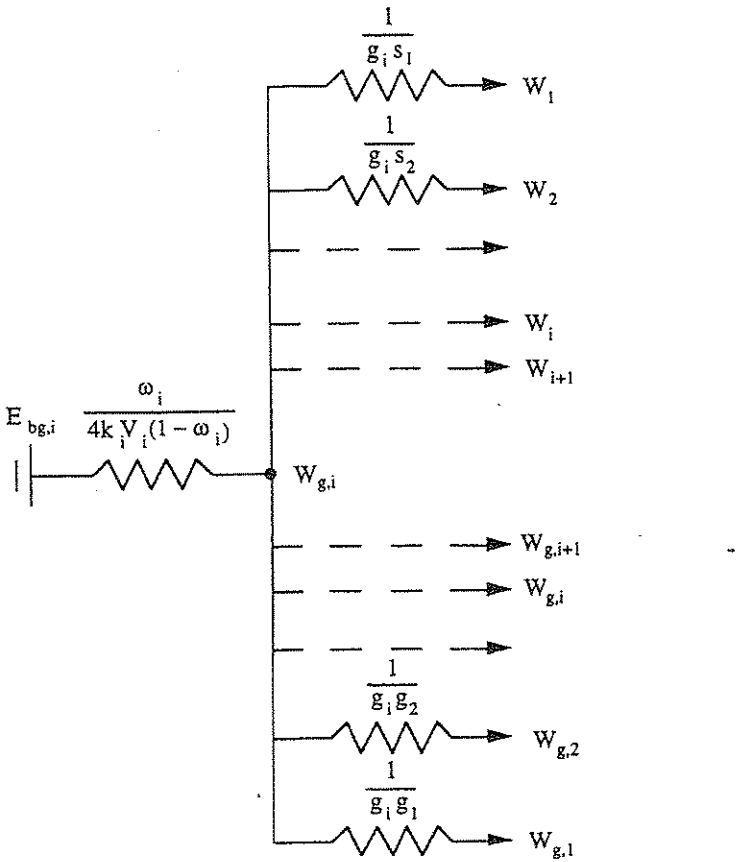

Figure 9 Network representation of a volume element V_i.

3.2 The Governing Equations

For the development of the governing equations, it is useful first to introduce the concept of irradiation, H_i and $H_{g,i}$, for a surface element A_i and a volume element V_i. Their physical interpretations are

$\frac{H_i}{\pi}$ = average intensity incident onto surface A_i

$\frac{H_{g,i}}{\pi}$ = average intensity incident into volume V_i

The consideration of energy balance at the surface element and volume element yields the following relation between the emissive power, radiosity, and irradiation

$$W_i = \varepsilon_i E_{b,i} + (1-\varepsilon_i) H_i \tag{21}$$

$$Q_i = A_i(W_i - H_i) = \frac{A_i\varepsilon_i}{1-\varepsilon_i}(E_{b,i} - W_i) \tag{22}$$

$$W_{g,i} = (1-\omega_i)E_{bg,i} + \omega_i H_{g,i} \tag{23}$$

$$S_{g,i} = 4k_iV_i\left(W_{g,i} - H_{g,i}\right) = 4k_iV_i\left(\frac{1-\omega_i}{\omega_i}\right)\left(E_{bg,i} - W_{g,i}\right) \tag{24}$$

The source terms Q_i and $S_{g,i}$ are the net radiative heat loss from surface A_i and net heat generation in volume V_i. They are analogous to "current" in an electrical network.

A second set of equations relating the different radiosities are generated by consideration of radiative exchange. Specifically, for an enclosure with N surface elements and M volume elements, the irradiation to a surface A_i and a volume V_i are given by

$$A_iH_i = \sum_{j=1}^{N}(s_is_j)W_j + \sum_{j=1}^{M}(s_ig_j)W_{g,j} \tag{25}$$

$$4k_iV_iH_{g,i} = \sum_{j=1}^{N}(g_is_j)W_j + \sum_{j=1}^{M}(g_ig_j)W_{g,j} \tag{26}$$

Using the following summation rules for the exchange factor

$$A_i = \sum_{j=1}^{N}(s_is_j) + \sum_{j=1}^{M}(s_ig_j) \tag{27}$$

$$4k_iV_i = \sum_{j=1}^{N}(g_is_j) + \sum_{j=1}^{M}(g_ig_j) \tag{28}$$

Eqs. (25) and (26), together with the first half of Eqs. (22) and (24) can be combined to yield

$$Q_i = \sum_{j=1}^{N}(s_is_j)(W_i - W_j) + \sum_{j=1}^{M}(s_ig_j)(W_i - W_{gj}) \tag{29}$$

$$S_{gi} = \sum_{j=1}^{N}(g_is_j)(W_{gi} - W_j) + \sum_{j=1}^{M}(g_ig_j)(W_{gi} - W_{gj}) \tag{30}$$

Eqs. (21) to (30) constitute the complete set of mathematical relations for the zonal method. In general, either Q_i ($S_{g,i}$) or $E_{b,i}$ ($E_{bg,i}$) are specified on each surface (volume) element. Eqs. (21) to (30) can be readily combined to yield the following general matrix equation for the unknown radiosity vector $\vec{W}$ ($W_1, W_2, \ldots, W_N, W_{g,1}, W_{g,2}, \ldots, W_{g,M}$)

$$\vec{W} = \bar{X}\vec{J} + \bar{Y}\vec{W} \tag{31}$$

Where $\bar{X}$ is a NM by NM diagonal matrix whose components are functions of ε_i, ω_i, k_i, A_i and V_i and $\bar{Y}$ is a NM by NM "full" matrix whose components are the various exchange factors. The components of the source vector $\vec{J}$ are either specified emissive power or surface heat loss (volumetric heat generation). The solution to Eq. (31) can be obtained by matrix inversion.

3.3 Application to Nongray Problems and Combined Mode Problems

Over the years, the inability to provide accurate quantitative analysis of radiative transfer in nongray media has been a primary obstacle in practical applications. A survey of the existing works show that there are two general approaches to the nongray problem. First, a great deal of effort has been exerted to identify the appropriate "mean" absorption coefficient (e.g., Planck mean, Rosseland mean, etc.) to extend the gray analysis to nongray applications. The success of these efforts, however, is quite limited, particularly for gaseous media. The second approach is to perform a direct line-by-line integration of the gray result. In general, this approach is considered inappropriate for practical applications because of the intensive computational requirement.

Even with the advance of modern computers, a line-by-line integration of the gray result using the "exact" absorption coefficient of gases is still extremely intensive computationally and probably not suitable for practical applications. However, for many practical engineering problems, particularly in combustion, there is no need to simulate the detailed line structure, and it is sufficient to use approximate expressions that exhibit the correct band-like behavior of gaseous absorption. The narrow-band fixed-line-spacing model [13] is an example of such approximation. Based on this approximation, the extension of the zonal method to nongray problem can be readily achieved by numerical integration of tabulated gray results. For a homogeneous medium, a schematic of the approach is shown in Figure 10. In a series of recent work [14–16], this approach is shown to be computationally efficient and accurate in generating heat transfer results in homogeneous nongray absorbing, emitting, and isotropically scattering media. If the computational domain consists of only a finite number of nongray subregions, the approach can be readily extended and is computationally feasible. Extension to general nongray

inhomogeneous media (or when the number of nongray subregions becomes large) is quite promising in view of the rapid advances achieved recently in large-scale computational data storage and retrieval.

It is important to note that the schematic in Figure 10 represents, fundamentally, an efficient way to "decouple" the geometric and optical aspects of the radiative heat transfer in practical systems. For a specific furnace in which the nongray subregions can be identified, the zonal calculation is needed to perform only once to generate the relevant heat transfer data over the expected range of radiative properties within each subregion. The data contain all the geometric effects that are characteristics for the considered furnace. Once these data are generated, a practicing engineer can then perform the spectral integration using the relevant radiative properties to obtain the required heat generation or temperature distribution for a specific application (either in a stand-alone or combined-mode calculation).

Historically, the zonal method has been perceived as difficult to use in a combined-mode problem. However, with the advance in modern computers and the possibility of parallel computing, this issue is close to being resolved. Because computer codes for conduction/convection analysis are readily available, the most effective way to deal with the combined mode problem is to use parallel computing to couple a conduction/convection analysis with a radiation analysis (e.g., using the zonal method), as shown schematically in Figure 11. There is no need for any additional research effort for the combined mode calculation except to resolve the various efficiency and accuracy issues related to the parallel computing process.

3.4 Summary

The governing equations for the zonal method is presented. These equations are applicable for general nonisothermal, inhomogeneous, absorbing, emitting, and isotropically

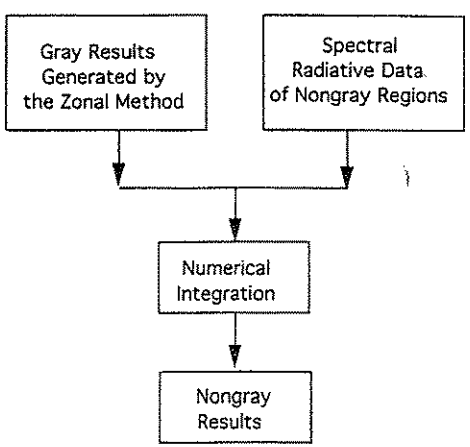

Figure 10 Schematic of a nongray calculation using the zonal method.

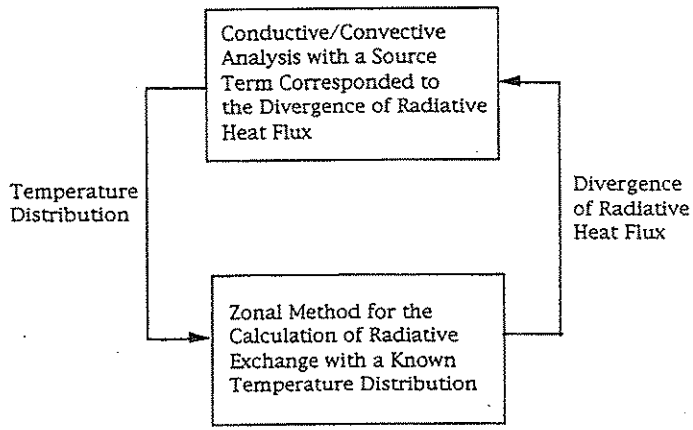

Figure 11 Schematic of a parallel computation algorithm using the zonal method.

scattering media. The formulation is analogous to the analysis of an electrical network. The nongray effect can be simulated by direct integration of tabulated gray results generated by the zonal method. This approach is feasible computationally when the computational domain consists of only a small finite number of nongray subregion. When the number of nongray subregion is large, the method requires the development of an efficient scheme for large-scale data storage and retrieval. The combined-mode problem is observed to be most efficiently solved by parallel computation using the zonal method as one component of the parallel processes.

4 ILLUSTRATIVE EXAMPLES OF APPLICATIONS

Examples are presented in this section that demonstrate the capability of the zonal method as described in the previous sections. The first example illustrates the nongray solution approach in a homogeneous, isothermal scattering medium. The second example illustrates the nongray solution approach in a three-dimensional enclosure with one nongray subregion. The third set of examples illustrates the usage of the zonal method to simulate the effect of a highly absorbing region (i.e., an opaque obstruction). The relative accuracy of using interpolated values from the table of generic normalized exchange factors in Appendix A in a radiative exchange calculation is also demonstrated.

4.1 Optical Properties Used in the Nongray Examples

In the first two examples, the nongray medium is assumed to be a mixture of gas and soot. For the gaseous absorption coefficient, the narrow-band fixed-line-spacing model [13], which is known to be an effective engineering approximation for the

nongray spectral absorption behavior for most common gases, is utilized. The gaseous absorption coefficient (suppressing the subscript λ for simplicity) is given by

$$a_g = \frac{\rho C^2 \sinh\left(\pi B^2 P_e/2\right)}{\cosh\left(\pi B^2 P_e/2\right) - \cos(2\pi\nu^*/d)} \tag{32}$$

where ν^* is the wavenumber measured from the center of the band, $C^2(\nu,T)$, $B^2(\nu,T)$, d, and Pe are specified in terms of isothermal gas correlation parameters as

$$C^2 = \left(C_1/C_3\right)e^{-\nu^*/C_3} \tag{33}$$

$$B^2 = C_2^2/\left(4C_1C_3\right) \tag{34}$$

$$d = d_0 C_3\left(T_0\right), \quad T_0 = 100K \tag{35}$$

$$P_e = \left[\left(P_B + bP_A\right)/P_0\right]^n, \quad P_0 = 1 \ atm \tag{36}$$

with P_A being the partial pressure of the absorbing gas and P_B the partial pressure of the N_2 broadening gas. The gas correlation parameters, C_1, C_2, C_3, b and n are defined for various common gaseous species (e.g., CO_2, H_2O, CO, and CH_4) in standard references [17].

For soot particles, the optical properties of carbon sphere is used. The absorption and extinction cross-section are evaluated using Mie Theory [18]. Specifically, for the set of index of refraction (n–ik) data for graphite carbon [19] as shown in Figure 12, the

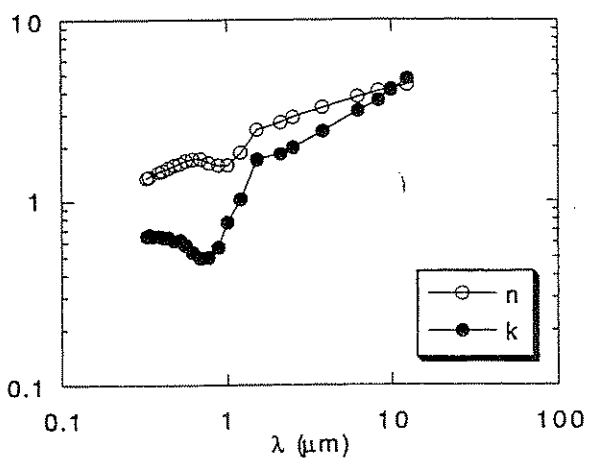

Figure 12 Measured data on the complex index of refraction (n–ik) for carbon.

absorption efficiency, Q_{abs}, the extinction efficiency, Q_{ext}, and scattering albedo, $\omega = 1 - \frac{Q_{abs}}{Q_{ext}}$, are calculated for different particle sizes utilizing computer programs provided in standard references [20]. The absorption coefficient, a_p, and extinction coefficient, k_p, can be generated from these efficiency factors by

$$a_p = N\pi r^2 Q_{abs} \quad k_p = N\pi r^2 Q_{ext} \tag{37}$$

with N being the particle's number density and r the particle radius. Typical numerical results are presented in Figure 13. It can be readily observed that the effect of scattering is quite significant when the particle radius is greater than 1 μm.

4.2 Nongray Radiative Transfer in an Isothermal Absorbing, Emitting, and Isotropically Scattering Medium (Concept of Absorption Mean Beam Length)

Because of the effect of scattering, the radiosity distribution in an isothermal enclosure is nonuniform and must be generated by a full numerical solution based on the zonal method. The detail of the solution is presented elsewhere [14–16]. For the convenience of physical interpretation and a direct comparison with the emittance of an isothermal nonscattering enclosure, the heat transfer results are expressed in terms of an absorption mean beam length (AMBL), $L_{ab,\lambda}$, as

$$q_\lambda\left(T_g, a_\lambda, w_\lambda\right) = E_{b,\lambda}\left(T_g\right)\left[1 - e^{-a_\lambda L_{ab,\lambda}}\right] \tag{38}$$

For a specific heat flux of interest, $q_\lambda(T_g,a_\lambda,w_\lambda)$, AMBL is the radius of an equivalent purely absorption hemisphere with the absorption coefficient, a_λ, such that the heat flux at the center of its base is identical to the actual heat flux. The subscript λ is retained in the definition of AMBL to emphasize that it is a function of wavelength because of its dependence on optical properties.

Numerical data of AMBL for a parallel slab radiating to its boundary are presented in Figure 14. For a gas/particle mixture, the total emittance can be expressed as a function of AMBL by

$$\varepsilon_{tot} = \varepsilon_p + \tau_p \varepsilon_g \tag{39}$$

with

$$\varepsilon_p = \frac{1}{\sigma T_g^4}\int_0^\infty E_{b,\lambda}\left(T_g\right)\left(1 - e^{-a_{p,\lambda}L_{ab,\lambda}\left(a_{t,\lambda},\omega_{t,\lambda}\right)}\right)d\lambda \tag{40}$$

and

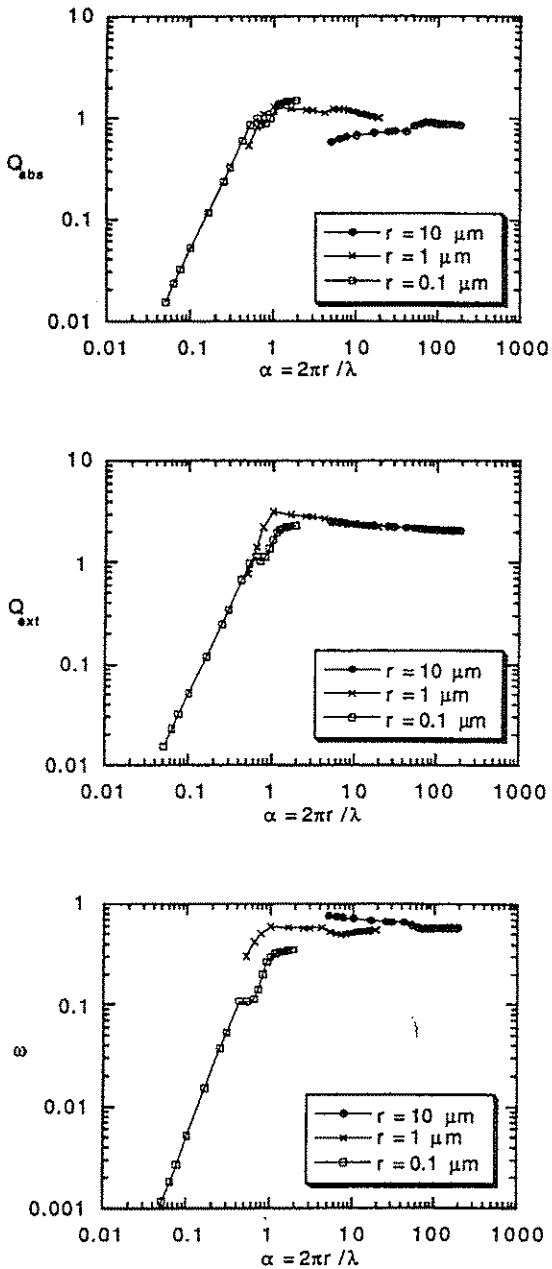

Figure 13 Absorption efficiency, extinction efficiency, and scattering albedo of carbon particles of different radius.

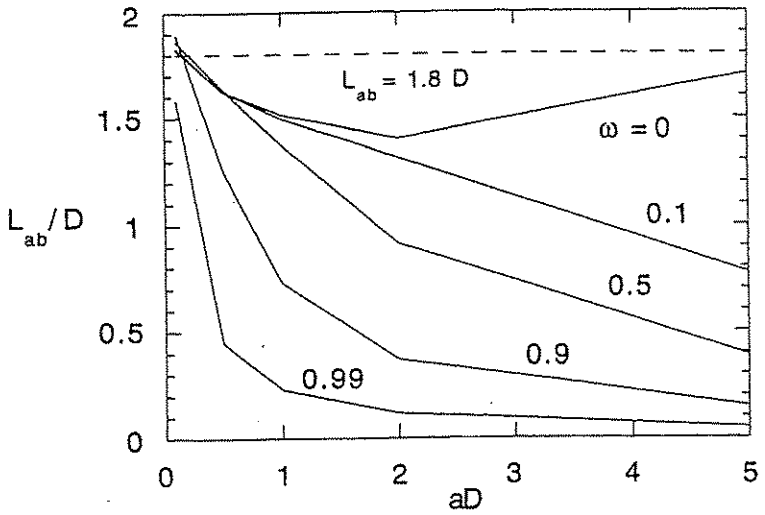

Figure 14 Ratio of absorption mean beam length to slab thickness for a parallel slab with different absorption optical thickness aD and scattering albedo ω.

$$\tau_p \varepsilon_g = \frac{1}{\sigma T_g^4} \int_0^\infty E_{b,\lambda}(T_g) e^{-a_{p,\lambda} L_{ab,\lambda}(a_{t,\lambda}, \omega_{t,\lambda})} \left(1 - e^{-a_{g,\lambda} L_{ab,\lambda}(a_{t,\lambda}, \omega_{t,\lambda})}\right) d\lambda \tag{41}$$

Physically, ε_p and $\tau_p \varepsilon_p$ represent the gas and particle contributions to the total mixture emittance, respectively. Because of the band-like absorption behavior of the gas, Eq. (41) can be further simplified by evaluating the AMBL at the center of each band and treated as a constant in the spectral integration across the band. This leads to

$$\tau_p \varepsilon_g = \frac{1}{\sigma T_g^4} \sum_i E_{b,\lambda_i}(T_g) e^{-a_{p,\lambda_i} L_{ab}(a_{p,\lambda_i} \omega_{p,\lambda_i})} \times \bar{A}_i \left[L_{ab}(a_{p,\lambda_i}, \omega_{p,\lambda_i}) \right] \tag{42}$$

where λ_i is the center of the ith band and $\bar{A}_i$ is the effective bandwidth given by

$$\bar{A}_i \left[L_{ab}(a_{p,\lambda_i}, \omega_{p,\lambda_i}) \right] = \int_{ithband} 1 - e^{-a_{g,\lambda} L_{ab}(a_{p,\lambda_i}, \omega_{p,\lambda_i})} d\lambda \tag{43}$$

Eq. (42) demonstrates the effectiveness of the AMBL concept. Because $\overline{A}_i$ for most common gases can be readily evaluated using established wide band correlations [17], the gaseous contribution to the total emittance in a multidimensional enclosure can be estim-ated from the AMBL results such as Figure 14 and one-dimensional band correlations.

To demonstrate the accuracy of the AMBL approach, the total mixture emittance and particle-attenuated gas emittance for a 1-meter slab of CO_2/particle mixture at a pressure of 1 atm are calculated by "integration" using Eqs. (40) and (41) and by "constant AMBL" using Eqs. (40) and (42). In the evaluation of Eq. (42), the Edward's wide band correlation [17] is used in the tabulation of the effective bandwidth, $\overline{A}_i$. The particle radius is varied from 0.1 μm to 10 μm to capture the effect of both a highly scattering particle cloud (with 10 μm radius) and a nonscattering particle cloud (with 0.1 μm radius). The particle concentration in each case is also varied to cover the range from a particle-dominated emittance (large concentration) to a gas-dominated emittance (low particle concentration). Results are presented in Figures 15, 16, and 17.

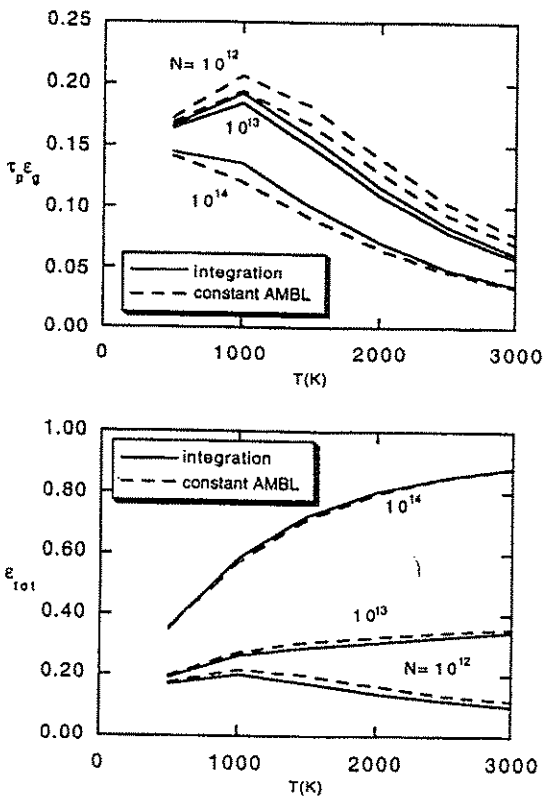

Figure 15 Comparison between the constant AMBL approach and the direct integration approach of the particle attenuated gas emittance and total emittance for a mixture with particle radius of 0.1 μm (N is the particle concentration in $1/m^3$).

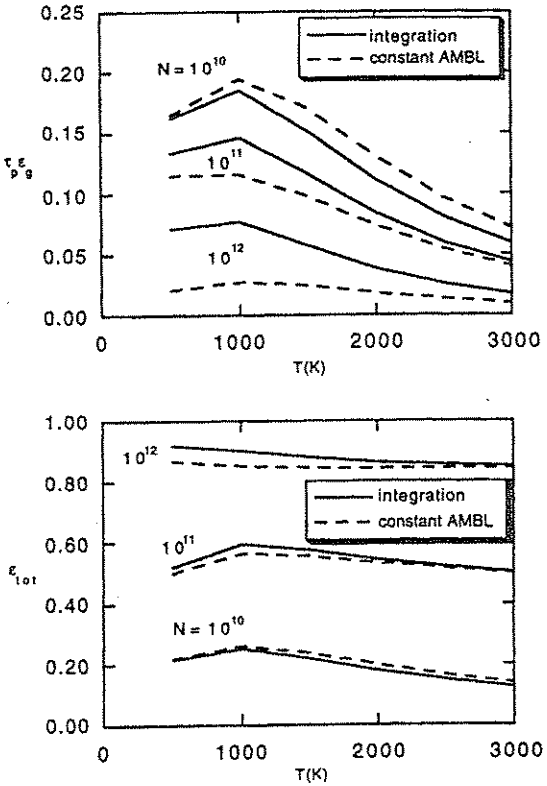

Figure 16 Comparison between the constant AMBL approach and the direct integration approach of the particle-attenuated gas emittance and total emittance for a mixture with particle radius of 1.0 μm (N is the particle concentration in $1/m^3$).

AMBL is clearly an effective parameter in summarizing the combined effect of the enclosure's geometry and scattering on the mixture's emittance. For a specific furnace of interest, AMBL can be tabulated by a zonal calculation and "stored" as a furnace's property. The emittance at arbitrary mixture's condition can then be calculated directly from Eq. (40) and (42).

4.3 Nongray Radiative Heat Transfer Simulation of a Hi-Rad Burner in An Industrial Furnace

The motivation of this illustrative example is to study the effect of a Hi-Rad burner on the melting rate of a "typical" aluminum remelting process furnace. A Hi-Rad burner is a plasma-enhanced natural gas burner that is designed to control the soot concentration in a flame to increase its radiative emission [21]. The objective of the calculation is to demonstrate the potential benefit of a Hi-Rad burner in the geometry of an actual furnace.

A schematic of the furnace above the melting aluminum and the expected location of the flame generated by a Hi-Rad burner is shown in Figure 18. The Hi-Rad burner is designed to be installed on the side wall at a distance h above the aluminum surface. In the simulation, the flame generated by the burner is approximated as a rectangular column of dimension $L_y \times L_z$, extending across the full diameter of the furnace (i.e., $\frac{L_x^2}{4} = R_o^2 - \frac{L_y^2}{4}$). The wall of the furnace is assumed to be gray, diffuse with emissivity ε_w, and at constant temperature T_w. The flame is assumed to be an isothermal gas/soot mixture. The surrounding medium is assumed to be optically transparent.

The absorption coefficient of gas is given again by Eq. (32). Carbon particles generated in the flame are assumed to be sufficiently small such that the absorption behavior follows the Rayleigh limit of Mie Theory. The absorption coefficient is given by

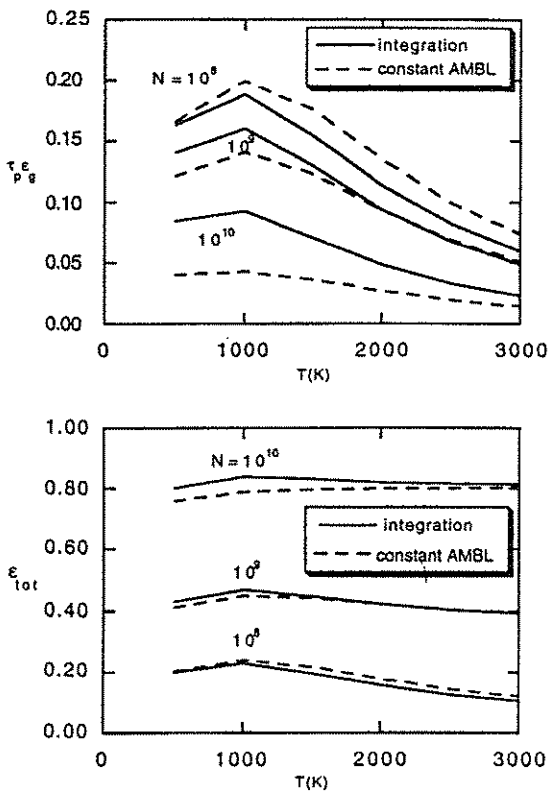

Figure 17 Comparison between the constant AMBL approach and the direct integration approach of the particle-attenuated gas emittance and total emittance for a mixture with particle radius of 10.0 μm (N is the particle concentration in 1/m³).

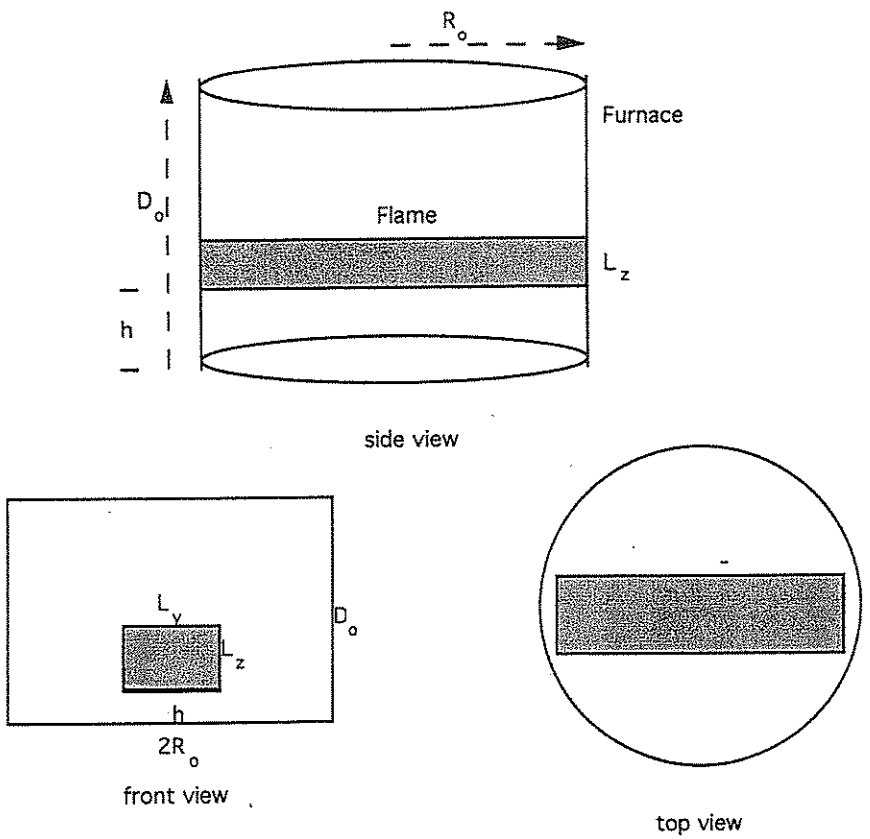

Figure 18 Geometry of the aluminum furnace and flame location.

$$a_\lambda = \frac{36\pi f_v}{\lambda} \frac{nk}{\left(n^2 - k^2 + 2\right)^2 + 4n^2k^2} \tag{44}$$

with $f_v = \frac{N\pi D^3}{6}$ being the volume fraction of carbon particles in the flame.

This example illustrates ideally the application of the zonal method to an inhomogeneous medium with the flame being a single nongray subregion (the wall is assumed to be gray). The AMBLs for the heat transfer to the various locations of the bottom surface are first tabulated as functions of the optical properties of the flame. The gray results are then integrated to yield the total heat transfer. The detail of the solution is presented elsewhere [21]. The effect of the soot concentration on the heat transfer from the flame, heat transfer from the top wall, heat transfer from the side wall and the total transfer to the bottom wall are shown in Figures 19 thru 22. The solutions show the effect of the soot in limiting the heat transfer from the side/top walls to the bottom

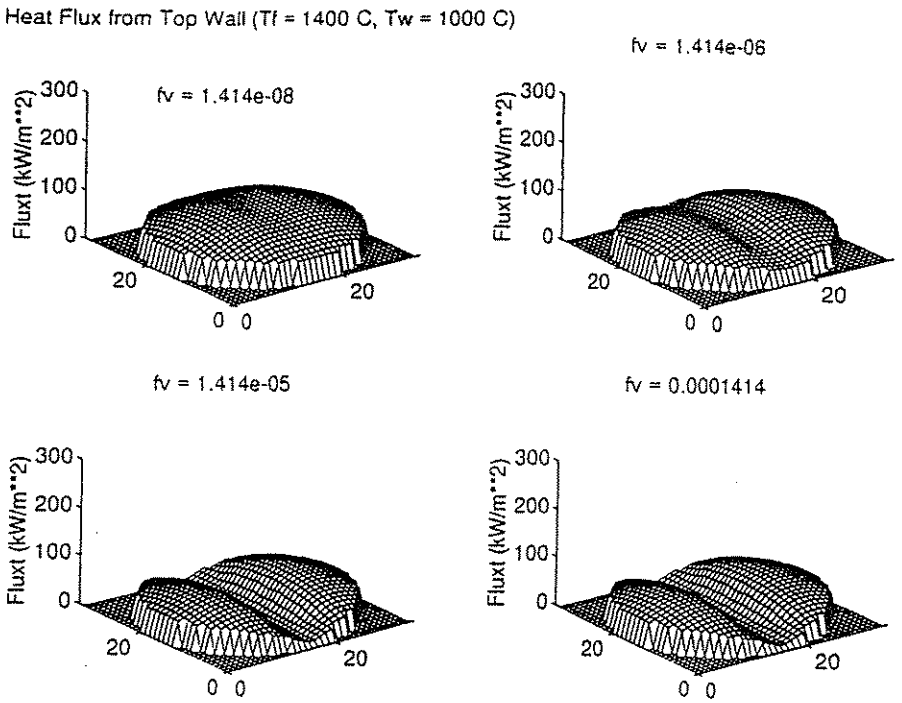

Figure 19 Radiative heat transfer from the top wall to the bottom wall at different soot volume fractions.

wall, as well as enhancing the emission of the flame. The capability of the zonal method in simulating these complex three-dimensional effects is quite apparent.

Inasmuch as the important physical parameter in this example is the radiative heat transfer distribution at the bottom (aluminum) surface, AMBL must be tabulated both as a two-dimensional function of spatial coordinates at the bottom surface and of optical properties of the flame. The data storage requirement is much more significant than that of the previous example. As both the number of nongray subregions and the level of detail of the heat flux distribution increase, the data storage requirement for AMBL multiplies rapidly. Thus, advances in large-scale data storage and retrieval are needed for this approach to be numerically feasible for general nongray problems. Nevertheless, many practical engineering problems can be modeled by a small number of nongray subregions, and the present method is a useful engineering approach.

4.4 Simulation of the Effect of Obstructions

The objective of this set of examples is to demonstrate the capability of zonal method in simulating the effect of an inhomogeneous medium, including the presence of an obstruction. The basic geometry is a cubical enclosure. Three separate cases are presented to illustrate the various aspects of the zonal method.

4.4.1 A Cubical Enclosure in Radiative Equilibrium. In this example, the relative accuracy of a zonal calculation using interpolated values of the exchange factor generated by the table of generic exchange factors in Appendix A is assessed. Specifically, a cubical furnace with black walls and dimension W is considered. The general geometry of this example and the notation used in the identification of elements for a $5 \times 5 \times 5$ calculation are shown in Figure 23. In the calculation, the walls with $z = 0$, $y = 0$ or $x = W$ have unit emissive power and the remaining walls are cold. For an optical dimension of 1.0, normalized exchange factors with $kD = 0.2$ are required for the calculation. Numerical data generated by the "exact" normalized exchange factors and those generated by linear interpolation between exchange factors with $kD = 0.1$ and $kD = 0.5$ are shown in Table 1. The "exact" results are identical to those generated independently by a previous investigation [10]. Because the change in exchange factors from $kD = 0.1$ to $kD = 0.5$ is quite significant, the agreement between the "interpolated" and the "exact" results is quite satisfactory. This comparison readily demonstrates that a zonal calculation using the table of generic normalized exchange factor is an effective approach, particularly for engineering applications.

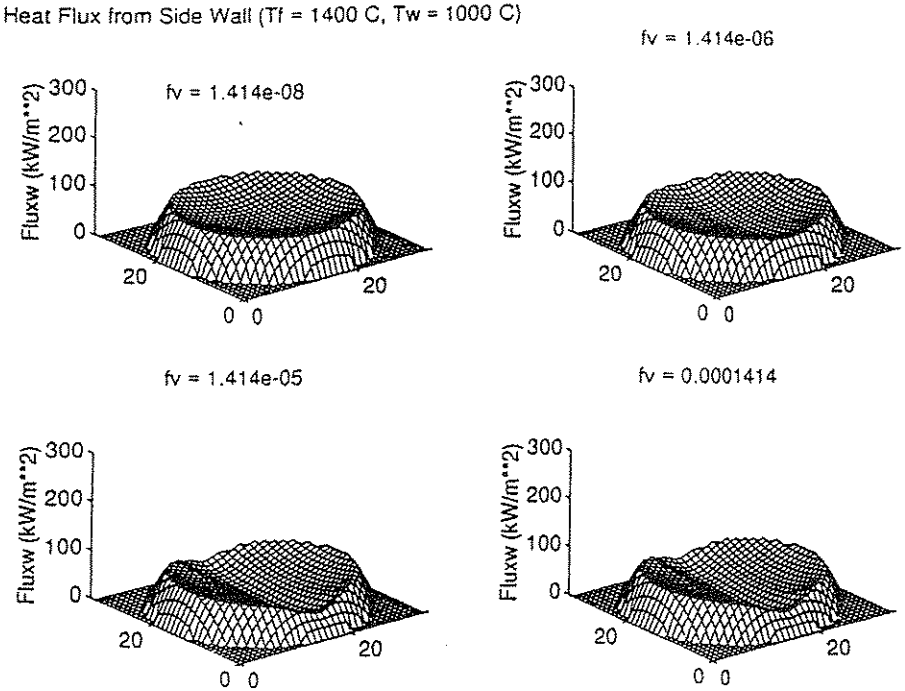

Figure 20 Radiative heat transfer from the side wall to the bottom wall at different soot volume fractions.

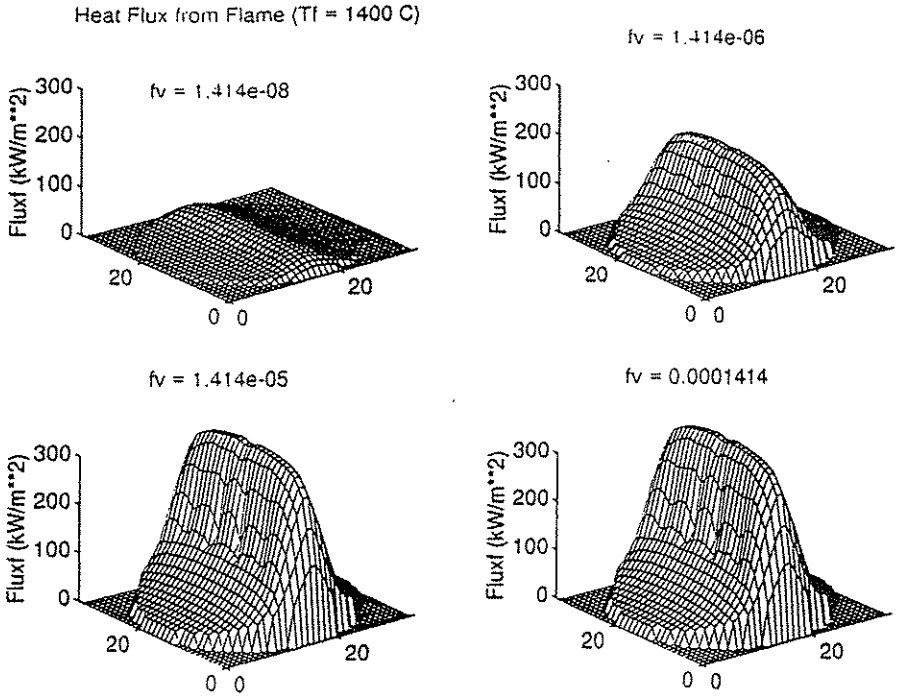

Figure 21 Radiative heat transfer from the flame to the bottom wall at different soot volume fractions.

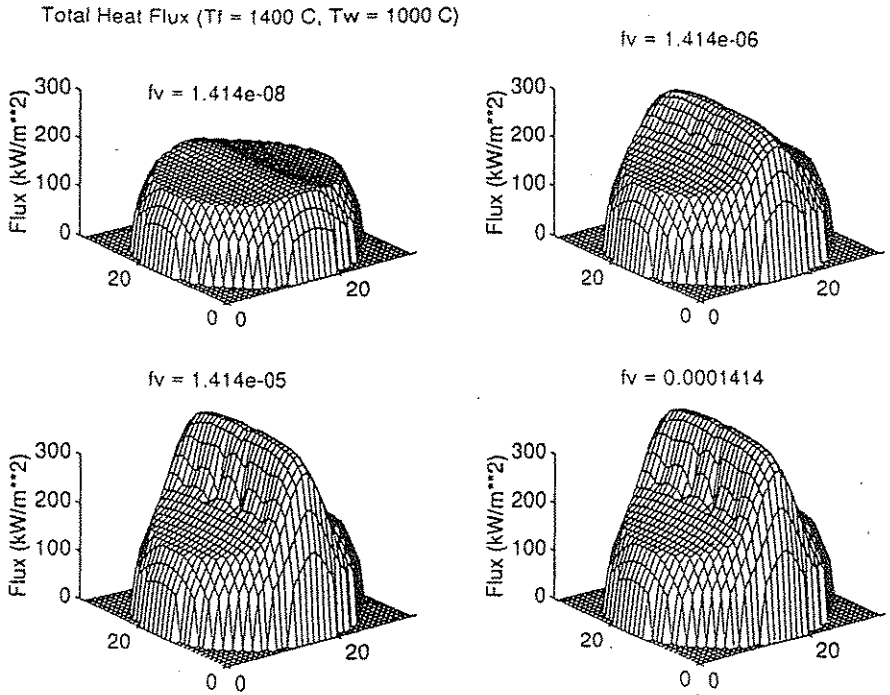

Figure 22 Total radiative heat transfer to the bottom wall at different soot volume fractions.

4.4.2 A Cubical Enclosure with a Radiating Flame. In this example, an emitting and scattering "flame" is situated in the middle of the furnace. Its relative locations and dimensions are shown in scale by Figure 24. The flame has a square cross-section of dimension $0.6\,W \times 0.6\,W$ and a height of $0.4\,W$. It is further separated into an inner and outer section. The inner section has a dimension of $0.2\,W \times 0.2\,W$ and a height of $0.4\,W$. The six surrounding walls are identified numerically as shown in the figure. Calculations are carried out for three sets of optical properties for the flame and the medium as shown in Table 2. In case a, a nonscattering flame is surrounded by a nonparticipating medium. In case b, the surrounding medium is an absorbing and scattering medium in radiative equilibrium. In case c, the flame is separated into a hotter nonscattering inner flame and a cooler absorbing/scattering outer flame surrounded by an absorbing and scattering medium in radiative equilibrium. The emissive power of the inner flame is normalized to be one and the emissive power of the outer flame in case c is 0.8.

To illustrate the accuracy and convergence of the zonal method, calculations are carried out for both a $5 \times 5 \times 5$ and a $10 \times 10 \times 10$ grid. Exchange factors are generated from interpolation of the generic normalized exchange factor table in Appendix A. Total heat transfer to the different walls, $Q(i)$, net heat loss from the flame, Q_m, and the overall energy balance, *Error*, for all cases are shown in Table 3. Note that in cases b and c, Q_m

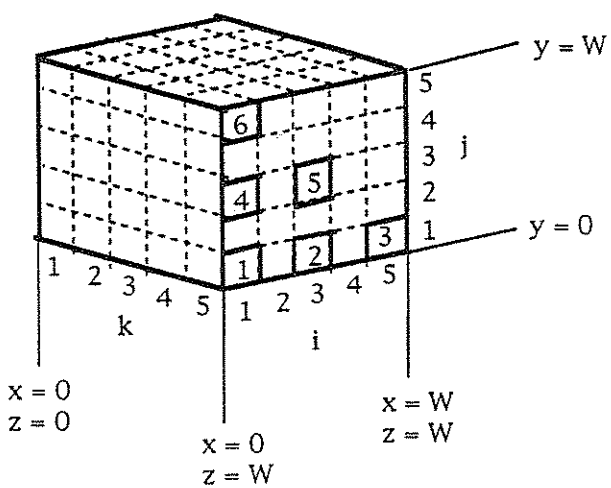

Figure 23 Geometry and notation used in the example of a cubical furnace in radiative equilibrium.

Table 1 Numerical Data for the Cubical Enclosure Problem. Values in Parenthesis Correspond to Results Generated By Interpolation of Data From the Table of Exchange Factors

		Emissive power				Heat flux
k	j	i = 1	i = 3	i = 5	Area	Q
5	5	0.105 (0.128)	0.177 (0.200)	0.368 (0.376)	1	0.499 (0.509)
5	3	0.177 (0.200)	0.298 (0.317)	0.500 (0.500)	2	0.695 (0.685)
5	1	0.368 (0.376)	0.500 (0.500)	0.632 (0.624)	3	0.822 (0.804)
					4	0.290 (0.326)
3	5	0.177 (0.200)	0.298 (0.317)	0.500 (0.500)	5	0.481 (0.500)
3	3	0.298 (0.317)	0.500 (0.500)	0.702 (0.683)	6	0.176 (0.214)
3	1	0.500 (0.500)	0.702 (0.683)	0.823 (0.800)		
1	5	0.368 (0.376)	0.500 (0.500)	0.632 (0.624)		
1	3	0.500 (0.500)	0.702 (0.683)	0.823 (0.800)		
1	1	0.632 (0.624)	0.823 (0.800)	0.895 (0.872)		

is less than the actual heat loss from the flame because it includes the absorption of the emission from the surrounding medium. The parameter *Error* in the table is defined by

$$Error = \left| \frac{\sum_{i=1}^{6} Q(i)}{Q_m} - 1 \right| \times 100 \tag{45}$$

The accuracy of the results and the effectiveness of the zonal method in capturing the essential heat transfer behavior are quite apparent.

4.4.3 A Cubical Enclosure with a Radiating Flame and an Opaque Obstruction. To demonstrate the capability of the zonal method in simulating the effect of an opaque obstruction, an obstacle is inserted into the furnace with geometry as shown in Figure 25. Computationally, the opaque obstruction is modeled as highly absorbing nonscattering volume elements with zero-emissive power. The total heat transfers to the different wall, the heat loss from the medium, and the overall energy balance are shown in Table 4. Note that in these cases, Q_m includes the absorption by the obstruction (it is treated as part of the surrounding medium) and therefore is less than the corresponding values in Table 3. As expected, the heat transfer to walls 2, 3, and 6 are greatly reduced due to the shadowing effect. The effect on $Q(1)$ and $Q(4)$ is much less because only a small fraction of the lines of sight between the flame and the walls are affected by the obstruction. In case a, heat transfer to the lower wall, $Q(5)$, is unaffected by the obstruction because the surrounding medium is nonparticipating. In cases b and c, $Q(5)$ is slightly reduced because part of the radiation reemitted by the medium is obstructed. To further illustrate the effectiveness of the zonal method

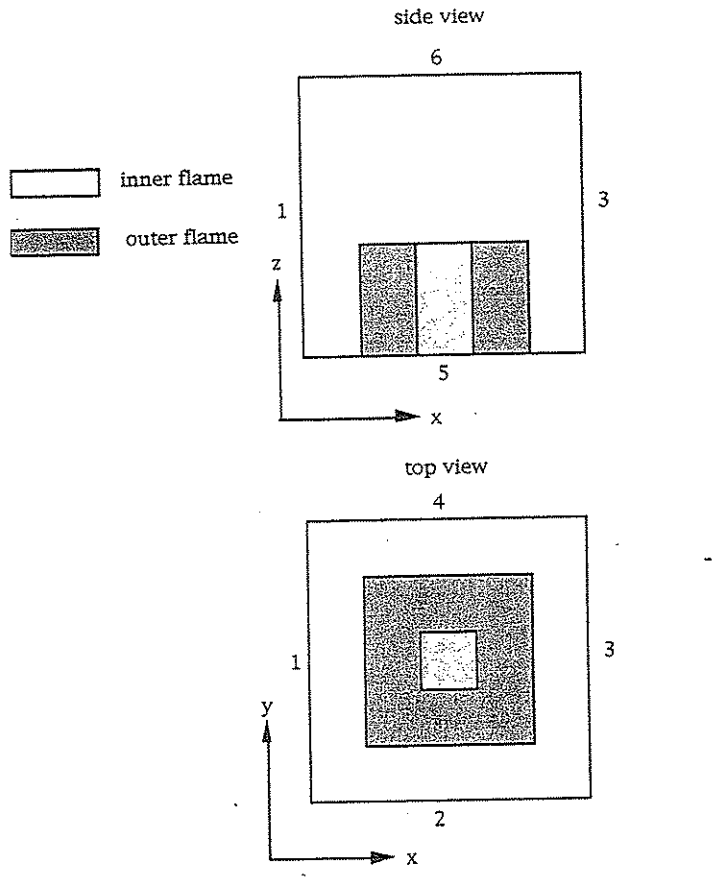

Figure 24 Geometry and notation used in the example of a cubical furnace with an emitting flame.

in the simulation of the effect of an obstruction, heat transfer distributions at walls 2 and 6 for case a, with and without the obstacle, are compared in Figure 26.

Table 2 Optical Properties of the Three Regions in the Problem of a Radiating Flame in a Cubical Enclosure

	Inner flame			Outer flame			Medium	
Case	*kW*	ω	*E*	*kW*	ω	*E*	*kW*	ω
a	2.5	0	1	2.5	0	1	0	0
b	2.5	0	1	2.5	0	1	0.5	0.3
c	2.5	0	1	2.5	0.5	0.8	0.5	0.3

Table 3 Numerical Data for a Cubical Enclosure with a Radiating Flame. Results Are Generated By a $10 \times 10 \times 10$ Grid, While Those in Parenthesis Are Generated By a $5 \times 5 \times 5$ Grid

Case	Q(1)	Q(5)	Q(6)	Q_m	Error(%)
a	3.171	7.085	2.027	21.87	0.33
	(3.043)	(7.086)	(1.994)	(21.66)	(1.87)
b	3.139	7.313	1.806	21.56	0.53
	(3.045)	7.330)	(1.791)	(21.37)	(0.33)
c	1.723	4.085	1.021	11.92	0.65
	(1.682)	(4.118)	(1.016)	(11.87)	(0.08)

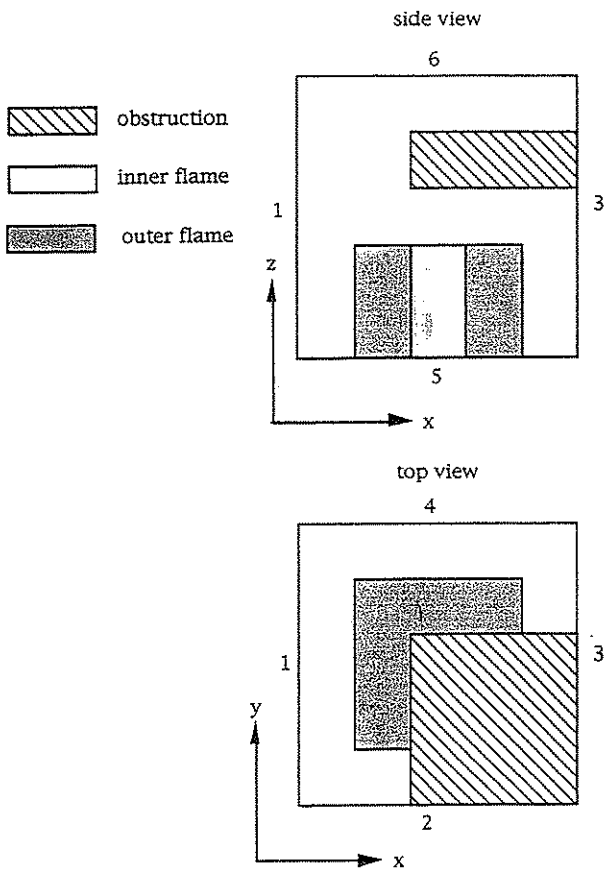

Figure 25 Geometry and notation used in the example of a cubical furnace with an emitting flame and an opaque obstruction.

Table 4 Numerical Data for a Cubical Enclosure with a Radiating Flame and an Obstacle. Results Are Generated by a $10 \times 10 \times 10$ Grid, While Those in Parenthesis Are Generated by a $5 \times 5 \times 5$ Grid

Case	Q(1)	Q(2)	Q(5)	Q(6)	Q_m	Error(%)
a	3.167	2.760	7.085	0.9601	19.89	0.00
	(3.043)	(2.665)	(7.086)	(0.9621)	(19.41)	(0.00)
b	3.098	2.706	7.297	0.8627	19.77	0.05
	(3.012)	(2.646)	(7.316)	(0.8298)	(19.47)	(0.05)
c	1.700	1.479	4.075	0.4830	10.92	0.05
	(1.664)	(1.456)	(4.109)	(0.4664)	(10.82)	(0.05)

4.5 Summary

The group of numerical examples presented in this section readily demonstrate the flexibility and capability of the zonal method in applications to complex engineering problems. Using the tables of generic normalized exchange factor, the computational requirement for these calculations (both in terms of computer time and data storage) are minimal.

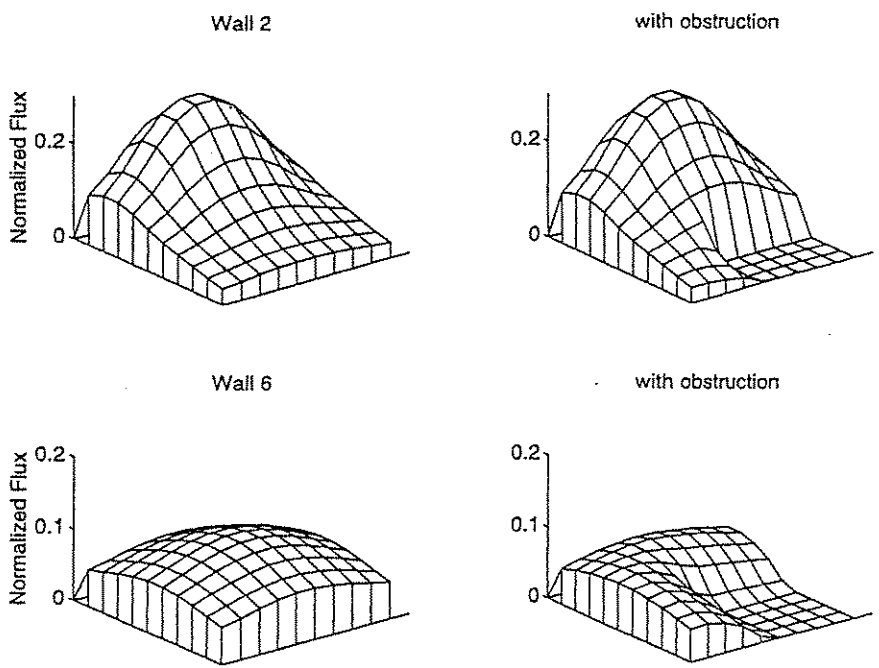

Figure 26 Effect of the obstruction on the heat transfer to walls 2 and 6 for case a.

5 EXTENSION OF THE ZONAL METHOD TO ANISOTROPICALLY SCATTERING MEDIUM: THE GENERALIZED ZONAL METHOD

The most severe limitation of the zonal method (called the conventional zonal method, CZM, in the remainder of this section) is the assumption that the volume radiosity, W_{gi}, and surface radiosity, W_i, are isotropic. This restricts the application of CZM to enclosures with diffuse surfaces and isotropically scattering media. In a recent work [22], this restriction is removed by the introduction of the generalized zonal method (GZM).

In this section, a detailed mathematical description of the GZM is presented. Formally, the GZM can be considered a vector generalization of the radiosity-irradiation approach utilized by CZM. The basic conservation equations for the GZM are derived. The concepts of average reflectivity and scattering phase function are introduced. These concepts characterize the scattering property of the medium and the reflecting property of the enclosed surface, respectively. Finally, the computational requirement for GZM is discussed and some approximate results generated with relatively large grid size are presented to illustrate the capability of the method.

5.1 The GZM Concepts of Radiosity Vector, Average Reflectivities, and Average Phase Functions

In an anisotropically scattering medium, an effective solution method must account for the directional dependence of the radiative intensity (and, therefore, the radiosity) in the medium. The fundamental basis of GZM is to let the level of discreteness in the computation control the level of detail in the simulation of the directional dependence of the radiosity in the calculation. As the level of discreteness increases, the simulation of the directional dependence becomes increasingly accurate, along with the predicted numerical solutions.

Specifically, in an enclosure with M volume zones and N surface zones, the method assumes that the radiosity from each zone is represented by a vector of NM components. For example, $W_{i,j}$ and $W_{i,gj}$ are the average radiosities from area A_i to area A_j and volume V_j. Likewise, $W_{gi,j}$ and $W_{gi,gj}$ are the average radiosities from volume V_i to area A_j and volume V_j. Each component of the radiosity vector is assumed to be constant in the evaluation of radiative exchange between elements. As the number of zones increase the directional dependencies of radiosity will be better simulated and the accuracy of numerical results will be improved.

Mathematically, the average irradiation incident onto surface A_i and volume V_i (Eqs. (25) and (26) for CZM) are now given by

$$A_i H_i = \sum_{j=1}^{N} \left(s_i s_j\right) W_{j,i} + \sum_{j=1}^{M} \left(s_i g_j\right) W_{gj,i} \quad i = 1, N \tag{46}$$

$$4kV_i H_{gi} = \sum_{j=1}^{N} \left(g_i s_j\right) W_{j,gi} + \sum_{j=1}^{M} \left(g_i g_j\right) W_{gj,gi} \quad i = 1, M \tag{47}$$

The heat transfers (Eqs. (29) and (30)) become

$$Q_i = \sum_{j=1}^{N} \left(s_i s_j\right)\left(W_{i,j} - W_{j,i}\right) + \sum_{j=1}^{M} \left(s_i g_j\right)\left(W_{i,gj} - W_{gj,i}\right) \quad i = 1, N \tag{48}$$

and

$$S_{gi} = \sum_{j=1}^{N} \left(g_i s_j\right)\left(W_{gi,j} - W_{j,gi}\right) + \sum_{j=1}^{M} \left(g_i g_j\right)\left(W_{gi,gj} - W_{gi,gi}\right) \quad i = 1, M \tag{49}$$

The radiosity vectors $\vec{W}_i$ and $\vec{W}_{gi}$ are related by the scattering properties of the medium and the reflective properties of the surfaces. The components of $\vec{W}_i$, radiosity vector of surface zone A_i, are written as

$$W_{i,j} = \varepsilon_i E_{b,i} + \frac{\pi}{A_i} \sum_{k=1}^{N} W_{k,i} \hat{\rho}_{k,i,j} \left(s_k s_i\right) + \frac{\pi}{A_i} \sum_{l=1}^{M} W_{gl,i} \hat{\rho}_{gl,i,j} \left(g_l s_i\right) \quad j = 1, N \tag{50}$$

and

$$W_{i,gj} = \varepsilon_i E_{b,i} + \frac{\pi}{A_i} \sum_{k=1}^{N} W_{k,i} \hat{\rho}_{k,i,gj} \left(s_k s_i\right) + \frac{\pi}{A_i} \sum_{l=1}^{M} W_{gl,i} \hat{\rho}_{gl,i,gj} \left(g_l s_i\right) \quad j = 1, M \tag{51}$$

The average reflectivities at surface A_i, $\hat{\rho}_{k,i,j}$, $\hat{\rho}_{gl,i,j}$ and $\hat{\rho}_{gl,i,gj}$ are defined by

$$\hat{\rho}_{k,i,j} = \frac{A_i}{\left(s_k s_i\right)\left(s_i s_j\right)} \int_{A_j} \int_{A_i} \int_{A_k} \rho'' \left(\vec{r}_i, \theta_{ji}, \phi_{ji}, \theta_{ki}, \phi_{ki}\right) e^{-k\left(r_{ji} + r_{ki}\right)} \times \frac{\left(\vec{r}_{ji} \cdot \vec{n}_i\right)\left(\vec{r}_{ji} \cdot \vec{n}_j\right)\left(\vec{r}_{ki} \cdot \vec{n}_i\right)\left(\vec{r}_{ki} \cdot \vec{n}_k\right)}{\pi^2 r_{ji}^{\,4} r_{ki}^{\,4}} dA_k dA_i dA_j \tag{52}$$

$$\hat{\rho}_{gl,i,j} = \frac{A_j}{\left(g_l s_i\right)\left(s_i s_j\right)} \int_{V_l} \int_{A_i} \int_{A_j} \rho'' \left(\vec{r}_i, \theta_{ji}, \phi_{ji}, \theta_{li}, \phi_{li}\right) e^{-k\left(r_{ji} + r_{li}\right)} \times \frac{\left(\vec{r}_{ji} \cdot \vec{n}_i\right)\left(\vec{r}_{ji} \cdot \vec{n}_j\right)\left(\vec{r}_{li} \cdot \vec{n}_i\right)}{\pi^2 r_{ji}^{\,4} r_{li}^{\,3}} k dA_j dA_i dV_l \tag{53}$$

$$\hat{\rho}_{gl,i,gj} = \frac{A_i}{(g_l s_i)(s_i g_j)} \int_{V_l}\int_{A_i}\int_{V_j} \rho''\left(\vec{r}_i, \theta_{li}, \phi_{li}, \theta_{ji}, \phi_{ji}\right) e^{-k(r_{ji} + r_{li})} \times \frac{(\vec{r}_{ji} \cdot \vec{n}_i)(\vec{r}_{li} \cdot \vec{n}_i)}{\pi^2 r_{ji}^3 r_{li}^3} k^2 dV_l dA_i dV_j \tag{54}$$

where $\rho''(\vec{r}_i, \theta_{ji}, \phi_{ji}, \theta_{ki}, \phi_{ki})$ is the bidirectional reflectivity of A_i at $\vec{r}_i$ for radiation incident in the (θ_{ji}, ϕ_{ji}) direction and reflecting in the (θ_{ik}, ϕ_{ik}) direction.

Likewise, the components of $\vec{W}_{gi}$, radiosity vector of volume zone V_i, are

$$W_{gi,j} = (1 - \omega) E_{bg,i} + \frac{\omega}{4kV_i} \sum_{k=1}^{M} W_{k,gi} \hat{\Phi}_{k,gi,j} (s_k g_i) + \frac{\omega}{4kV_i} \sum_{l=1}^{N} W_{gl,gi} \hat{\Phi}_{gl,gi,j} (g_l g_i) \quad j = 1, N \tag{55}$$

$$W_{gi,gj} = (1 - \omega) E_{bg,i} + \frac{\omega}{4kV_i} \sum_{k=1}^{N} W_{k,gi} \hat{\Phi}_{k,gi,gj} (s_k g_i) + \frac{\omega}{4kV_i} \sum_{l=1}^{M} W_{gl,gi} \hat{\Phi}_{gl,gi,gj} (g_l g_i) \quad j = 1, M \tag{56}$$

where $\hat{\Phi}_{k,gi,j}$, $\hat{\Phi}_{gl,gi,j}$ and $\hat{\Phi}_{gl,gi,gj}$ are the average scattering phase functions given by

$$\Phi_{k,gi,j} = \frac{kV_i}{(s_k g_i)(g_i s_j)} \int_{A_j}\int_{V_i}\int_{A_k} \Phi(\cos\theta_{jik}) e^{-k(r_{ji} + r_{ki})} \times \frac{(\vec{r}_{ji} \cdot \vec{n}_j)(\vec{r}_{ki} \cdot \vec{n}_k)}{\pi^2 r_{ji}^3 r_{ki}^3} k dA_k dV_i dA_j \tag{57}$$

$$\Phi_{gl,gi,j} = \frac{kV_i}{(g_l g_i)(g_i s_j)} \int_{V_l}\int_{V_i}\int_{A_j} \Phi(\cos\theta_{jil}) e^{-k(r_{ji} + r_{li})} \times \frac{(\vec{r}_{ji} \cdot \vec{n}_j)}{\pi^2 r_{ji}^2 r_{li}^3} k^2 dV_l dV_i dA_j \tag{58}$$

and

$$\Phi_{gl,gi,gj} = \frac{kV_i}{(g_l g_i)(g_i g_j)} \int_{V_l}\int_{V_i}\int_{V_j} \Phi(\cos\theta_{jil}) e^{-k(r_{ji} + r_{li})} \times \frac{1}{\pi^2 r_{ji}^2 r_{li}^2} k^3 dV_l dV_i dV_j \tag{59}$$

In the above expressions, $\Phi(\cos\theta_{jik})$ is the phase function V_i at $\vec{r}_i$ for radiation incident in direction (θ_{ji}, ϕ_{ji}) and being scattered into the $(\theta_{ik}\phi_{ik})$ direction. The detailed derivation of Eqs. (53) and (58) are presented in Appendix B. Development of Eqs. (52), (54), (57), and (61) are similar.

Analogous to Eq. (31) for CZM, Eqs. (46), (47), (48), (49), (50), (51), (55), and (56) can be rewritten as a generalized matrix equation for the generalized radiosity vector $\tilde{\mathbf{W}}$ (composed of the vectors $\vec{W}_1, \vec{W}_2, \ldots, \vec{W}_N, \vec{W}_{g1}, \vec{W}_{g2}, \ldots, \vec{W}_{gM}$).

$$\tilde{\mathbf{W}} = \underline{\tilde{\mathbf{X}}}\tilde{\mathbf{J}} + \underline{\tilde{\mathbf{Y}}}\tilde{\mathbf{W}} \tag{60}$$

where $\underline{\tilde{\mathbf{X}}}$ is a diagonal *NM* by *NM* generalized matrix with elements that are *NM* by *NM* submatrices. The submatrix elements are functions of ε_i, ω, A_i and V_i. $\underline{\tilde{\mathbf{Y}}}$ is a full *NM* by *NM* generalized matrix composed of *NM* by *NM* submatrices. The submatrix elements of $\underline{\tilde{\mathbf{Y}}}$ are composed of the GZM average reflectivity factors or average scattering phase function factors and the CZM exchange factors. $\tilde{\mathbf{J}}$ is a generalized source vector composed of *NM* subvectors whose components are the specified emissive powers or heat fluxes.

From their definition, it is apparent that the average reflectivities and phase functions satisfy the following reciprocity relations

$$\hat{\rho}_{j,i,k} = \hat{\rho}_{k,i,j} \tag{61}$$

$$\hat{\rho}_{gj,i,k} = \hat{\rho}_{k,i,gj} \tag{62}$$

$$\hat{\rho}_{gj,i,gk} = \hat{\rho}_{gk,i,gj} \tag{63}$$

$$\hat{\Phi}_{j,gi,k} = \hat{\Phi}_{k,gi,j} \tag{64}$$

$$\hat{\Phi}_{gj,gi,k} = \hat{\Phi}_{k,gi,gj} \tag{65}$$

$$\hat{\Phi}_{gj,gi,gk} = \hat{\Phi}_{gk,gi,gj} \tag{66}$$

At a volume element V_i and relative to an arbitrary surface A_k or volume V_k, the average phase functions satisfy the closure relation

$$4kV_i = \sum_{j=1}^{N} (g_i s_j)\hat{\Phi}_{k,gi,j} + \sum_{l=1}^{M} (g_i g_l)\hat{\Phi}_{k,gi,gl}$$
$$= \sum_{j=1}^{N} (g_i s_j)\hat{\Phi}_{gk,gi,j} + \sum_{l=1}^{M} (g_i g_l)\hat{\Phi}_{gk,gi,gl} \quad (67)$$

Eqs. (46) to (67) represent a complete mathematical description of the radiative transfer based on the generalized zonal method. The description is completely general and is applicable to media with arbitrary scattering phase functions and surfaces with arbitrary bidirectional reflectivities. Even though the method requires the tabulation of the average phase functions and average reflectivities, which are complex multidimensional volumetric and area integration, it is important to note that these tabulations are needed to be carried out once for a given geometry, scattering phase function, and surface reflectivity. As in CZM, these factors can be expressed in generic normalized forms that are applicable for general enclosures and can account for the effect of inhomogenous properties.

5.2 An Illustrative Example of GZM

To demonstrate the effectiveness of the GZM, the problem of radiative equilibrium in a cubical enclosure containing an anisotropically scattering medium is analyzed. The specific geometry and coordinate system are shown in Figure 27. The bottom

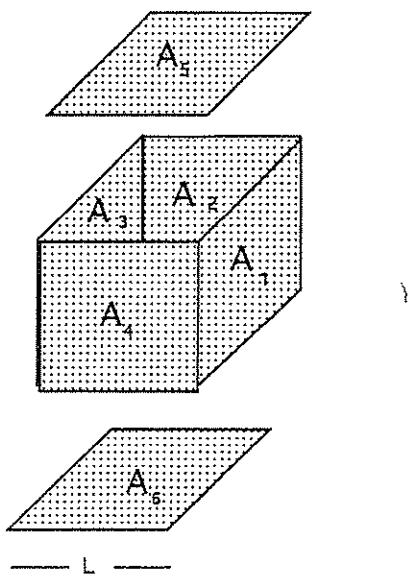

Figure 27 Geometry and notation used in the GZM example problem.

surface (A_6) is black and hot with a unit emissive power, while the remaining five surfaces are black and cold with zero emissive power. The medium has a linear anisotropic scattering phase function given by

$$\Phi(\theta) = 1 + \beta \cos\theta \quad (68)$$

The number of zones used in the analysis was progressively increased in order to prove convergence. The first analysis was with one volume zone ($n_z = 1$) for the entire medium and six surface zones, one for each wall. The next analysis used eight volume zones ($n_z = 2$; $2 \times 2 \times 2$ grid) and 24 surface zones. The final analysis used 64 volume zones ($n_z = 4$; $4 \times 4 \times 4$ grid) and 96 surface zones. It should be noted that the complexity of the analysis grows quite rapidly. It is shown later that the one volume zone analysis could be done in closed form. The eight volume zone analysis had 16 unknowns; the 64 zone analysis had 768 unknowns.

The presentation in this section is in two parts. In the first subsection the one-zone analysis is presented in detail. This illustrates some unique features of the GZM. In the second subsection, gridsize convergence is shown. More detailed discussion of the numerical data and the physics of the problem are presented elsewhere [22].

5.2.1 One Zone Analysis. In the one zone analysis the entire medium is treated as a single volume zone and each wall is a single surface zone. To simplify the notation, the subscript g is used for the single volume zone. Inasmuch as all surfaces are black, the radiosity on each surface is known (1 for A_6 and 0 for the remaining surfaces). From Eq. (48), the heat transfer at the six surfaces is given below.

$$Q_i = -(s_6 s_i) - (g s_i)\, W_{gi} \qquad i = 1, \ldots, 5 \quad (69)$$

and

$$Q_6 = 1 - (g s_6)\, W_{g,6} \quad (70)$$

The radiosity components for the gas zone can be deduced from Eq. (55) to yield

$$W_{g,j} = (1-\omega)E_{bg} + \frac{\omega}{4kV_g}\left(\hat{\Phi}_{6,g,j}(g s_6) + \hat{\Phi}_{g,g,j}(gg)W_{g,g}\right) \qquad j = 1, \ldots 6 \quad (71)$$

and

$$W_{g,g} = (1-\omega)E_{bg} + \frac{\omega}{4kV_g}\left(\hat{\Phi}_{6,g,g}(g s_6) + \hat{\Phi}_{g,g,g}(gg)W_{g,g}\right) \quad (72)$$

E_{bg}, the average emissive power of the medium, can be deduced from combining Eqs. (49) and (72) to be

$$E_{bg} = \frac{(s_6 g)\left[\left(1 - \frac{\omega}{4kV_g}(gg)\right)\left(\hat{\Phi}_{g,g,g} - \hat{\Phi}_{6,g,g}\right)\right]}{4kV_g - (gg) + \omega(gg)\left(1 - \hat{\Phi}_{g,g,g}\right)} \tag{73}$$

Eqs. (71) and (72) illustrate that the components of the radiosity vector, Wg,i, are not identical in general. While this is expected for anisotropically scattering media, it is true even for an isotropically scattering medium. This is a direct contradiction of CZM assumption that all components of the radiosity vector should be equal. This contradiction can be explained both physically and mathematically.

Physically, the imbalance reflects the anisotropic nature of the boundary conditions (unit emissive power at the bottom wall and zero emissive power elsewhere). For a single volume zone, it is clear that the radiosity components to the top wall and side walls cannot be equal.

Mathematically, the equations for radiosity components use the scattering factors to show the effects of geometry and scattering phase function. Note that even for an isotropic scattering medium, the scattering factor is unity only for a differential volume element dV_{gi}, i.e.,

$$\hat{\Phi}_{j,dgi,k} = \hat{\Phi}_{gj,dgi,k} = \hat{\Phi}_{gj,dgi,gk} = 1.0 \tag{74}$$

The scattering factors for a finite volume element, V_{gi}, on the other hand, are unequal and given by

$$\hat{\Phi}_{k,gi,j} = \frac{V_i}{(g_i s_k)(g_i s_j)} \int_{V_i} \frac{(s_j dg_i)(s_k dg_i)}{dV_i} \tag{75}$$

The difference in exchange factors led to the difference in the radiosity components. The difference in isotropic results disappears as the number of zones taken in the CZM and GZM analyses increases. However, for the same number of zones, GZM is clearly an improvement over CZM even for an isotropic analysis.

It is interesting to note that utilizing the appropriate summation rule for ex-change factors and scattering factors, Eq. (73) in the limit of a cubic enclosure, is reduced to

$$E_{bg} = \frac{1}{6} \tag{76}$$

This is the expected result from superposition and the same result as a one zone CZM analysis. This reaffirms that the difference between CZM and GZM is in the treatment of scattering. From examining Eqs. (71) and (72), it is clear that CZM and GZM are identical if there is no scattering ($\omega = 0$).

5.2.2 Convergence. To illustrate their effect on convergence, the optical thickness, scattering albedo, and scattering phase function were varied. Runs were made for optical thickness $L = 0.1, 0.5, 1.0, 2.0, 3.0$; scattering albedo $\omega = 0, 0.2, 0.4, 0.6, 0.8, 1$; and linear scattering coefficient $\beta = -1, 0, 1$. In order to show that GZM is an effective solution method, gridsize convergence must be shown.

In Tables 5 to 9, the bottom, side, and top wall fluxes $q_b = Q_6/L^2$; $q_s = -Q_1/L^2$; $q_t = -Q_5/L^2$ for various grids are shown. Results for $\omega = 1$ were chosen because they are "pure" GZM results; the results are entirely dominated by scattering. The tables show that the fluxes have converged to within 5% for the bottom and side walls and within 0.015 for the top wall (the top wall convergence is slow because of the small dimensionless heat flux). For L = 0.1, an optically thin case, only eight volume zones ($n_z = 2$) are necessary for convergence. For all other optical thicknesses 64 volume zones ($n_z = 4$) are required.

Table 5 Convergence Behavior of the Total Heat Flux Predictions Generated by GZM for an Optical Thickness of L = 0.1

	q_b		q_s		q_t	
β	$n_z = 1$	$n_z = 2$	$n_z = 1$	$n_z = 2$	$n_z = 1$	$n_z = 2$
−1	0.9808	1.0000	0.1990	0.2000	0.1866	0.2000
0	0.9890	1.0000	0.2000	0.2000	0.1890	0.2000
1	1.0000	1.0000	0.2017	0.2000	0.1909	0.2000

Table 6 Convergence Behavior of the Total Heat Flux Predictions Generated by GZM for an Optical Thickness of L = 0.5

	q_b		q_s		q_t	
β	$n_z = 2$	$n_z = 4$	$n_z = 2$	$n_z = 4$	$n_z = 2$	$n_z = 4$
−1	0.9016	0.8995	0.1964	0.1958	0.1299	0.1334
0	0.9300	0.9280	0.2004	0.1999	0.1422	0.1454
1	0.9590	0.9580	0.2045	0.2040	0.1552	0.1585

Table 7 Convergence Behavior of the Total Heat Flux Predictions Generated by GZM for an Optical Thickness of L = 1.0

	q_b		q_s		q_t	
β	$n_z = 2$	$n_z = 4$	$n_z = 2$	$n_z = 4$	$n_z = 2$	$n_z = 4$
−1	0.8299	0.8248	0.1872	0.1873	0.0897	0.0917
0	0.8730	0.8691	0.1943	0.1945	0.1046	0.1065
1	0.9171	0.9163	0.2014	0.2020	0.1208	0.1239

Table 8 Convergence Behavior of the Total Heat Flux Predictions Generated By GZM for an Optical Thickness of L = 2.0

	q_b		q_s		q_t	
β	$n_z = 2$	$n_z = 4$	$n_z = 2$	$n_z = 4$	$n_z = 2$	$n_z = 4$
−1	0.7390	0.7227	0.1722	0.1705	0.0537	0.0516
0	0.7938	0.7809	0.1829	0.1816	0.0666	0.0648
1	0.8497	0.8432	0.1935	0.1931	0.0810	0.0812

Table 9 Convergence Behavior of the Total Heat Flux Predictions Generated by GZM for an Optical Thickness of L = 3.0

	q_b		q_s		q_t	
β	$n_z = 2$	$n_z = 4$	$n_z = 2$	$n_z = 4$	$n_z = 2$	$n_z = 4$
−1	0.6809	0.6553	0.1597	0.1573	0.0389	0.0341
0	0.7442	0.7174	0.1721	0.1702	0.0487	0.0442
1	0.7978	0.7834	0.1844	0.1836	0.0596	0.0571

In Figure 28, the convergence behavior of a pure isotropic scattering ($\omega = 1$) GZM solution ($N_z = 1, 2, 4$) is shown and compared with the corresponding CZM results.

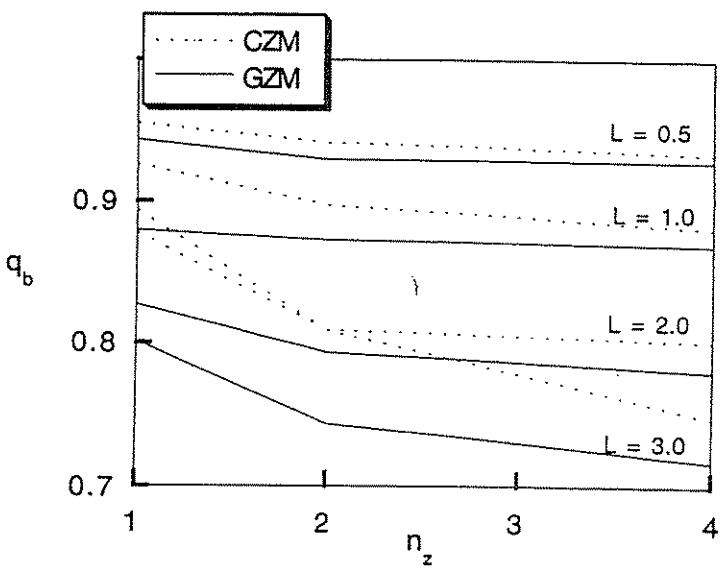

Figure 28 Convergence behavior of GZM and CZM for the isotropically scattering results.

These results represent numerical proof of the earlier statement that given the same number of zones GZM solutions are more accurate than CZM. This increased accuracy compensates for the increased effort required by the GZM.

Although total heat transfer results for the current illustrative example can be generated accurately with only 64 zones, solutions with a larger number of zones are required for more complex problems. Because the number of average scattering phase function factors and average reflectivity factors increases rapidly with the number of zones, the practical usage of GZM would require the utilization of parallel computing and/or advance techniques in large memory data storage and retrieval. These are areas of active current research. With the rapid advances in the fundamental understanding of computer science, these limitations are expected to be readily overcome in the near future, and GZM can become a practical solution technique for realistic radiative heat transfer simulation.

5.3 Summary

The basic mathematical formulation of GZM is presented. The capability of the method is demonstrated by the solution of a simple three-dimensional radiative heat transfer problem with anisotropic scattering. While the solution method of GZM is straightforward, a calculation with small grid size requires the utilization of parallel computing and some advances in large memory data storage and retrieval in practical calculations. With the rapid advances in computer science research, these obstacles are not significant, and GZM has good potential of becoming a practical solution approach for radiative heat transfer.

6 CONCLUDING REMARKS

A review of the zonal method is presented. The method is shown to be both accurate and efficient in the analysis of radiative heat transfer in nonisothermal inhomogeneous medium with isotropic scattering. A set of generic normalized exchange factors are tabulated. They can be used in problems with general three-dimensional rectangular geometry. Based on mathematical properties of these exchange factors, the conventional "diffusion" approximation in finite-difference form is shown to be inaccurate. A concept of "radiation length" is introduced to reduce slightly the complexity of the numerical implementation. Numerical examples are presented to demonstrate the capability of the method in simulating radiative heat transfer in inhomogeneous media, including the effect of opaque obstructions.

For media with anisotropic scattering, the method is extended to become the generalized zonal method. Solutions with a relatively small number of zones are presented to demonstrate the capability of the method. For problems that require small grid size, the method's capability is limited because of the large number of exchange factors that must be tabulated and the large size of the resulting matrix equation. With rapid advances in parallel computing and large memory data storage

and retrieval, these difficulties are expected to be eliminated soon and the generalized zonal method has an excellent potential of becoming a practical approach for the analysis of radiative transfer in practical engineering systems.

REFERENCES

1. H. C. Hottel, Radiant Heat Transmission, in *Heat Transmission,* (ed. W. H. McAdams), Ch. 4, McGraw-Hill, New York, 1954.
2. H. C. Hottel and E. S. Cohen, Radiant Heat Exchange in a Gas-Filled Enclosure: Allowance for Non-Uniformity of Gas Temperature, *AIChE Journal,* Vol. 4, No. 1, pp. 3–14, 1958.
3. H. C. Hottel and A. F. Sarofim, Gaseous Radiation with Temperature Gradients, Allowance for Isotropic Scatter, *Research in Heat Transfer,* Pergamon Press, Oxford, pp. 139–150, 1963.
4. H. C. Hottel and A. F. Sarofim, *Radiative Transfer* , McGraw-Hill, New York, 1967.
5. M. Q. Brewster, *Thermal Radiative Transfer and Properties,* John Wiley and Sons, New York, 1992.
6. R. Siegel and J. R. Howell, *Thermal Radiation Heat Transfer,* 3rd ed., Hemisphere Publishing, Washington, D. C., 1992.
7. D. K. Edwards and A. Balakrishnan, Volume Interchange Factors for Nonhomogeneous Gases, *ASME J. Heat Transfer,* Vol. 94, pp. 181–187, May 1972.
8. J. J. Noble, The Zonal Method: Explicit Matrix Relations for Total Exchange Areas, *Int. J. Heat and Mass Transfer,* Vol. 18, No. 2, pp. 261–269, Feb. 1975.
9. H. B. Becker, A Mathematical Solution for Gas-to-Surface Radiative Exchange Area for Rectangular Parallelepiped Enclosure Containing a Gray Medium, *ASME J. Heat Transfer,* Vol. 99, pp. 203–207, May 1977.
10. M. E. Larsen and J. R. Howell, The Exchange Factor Method: An Alternative Basis for Zonal Analysis of Radiating Enclosures, *ASME J. Heat Transfer,* Vol. 107, pp. 936–942, 1985.
11. R. J. Tucker, Direct Exchange Areas for Calculating Radiation Transfer in Rectangular Furnaces, *ASME J. Heat Transfer,* Vol. 108, pp. 707–710, 1986.
12. W. W. Yuen and A. Ma, On the Development of Approximation Methods for Radiative Heat Transfer, A Fundamental Limitation and the Utilization of the Radiation-Length Concepts, *Numberical Methods in Thermal Problems, Proceedings of the Seventh International Conference,* Vol. VII, Part 1, pp. 729–739, 1991.
13. D. K. Edwards, L. K. Glassen, W. C. Hauser, and J. S. Tuchscher, Radiative Heat Transfer in Nonisothermal Gases, *ASME J. Heat Transfer,* pp. 219–229, August 1967.
14. W. W. Yuen, Development of a Network Analogy and Evaluation of Mean Beam Length for Multi-Dimensional Absorbing/Isotropically Scattering Media, *ASME J. Heat Transfer,* Vol. 112, pp. 408–414, 1990.
15. W. W. Yuen and A. Ma, Evaluation of Total Emittance of an Isothermal Nongray Absorbing, Scattering Gas-Particle Mixture Based on the Concept of Absorption Mean Beam Length, *ASME J. Heat Transfer,* Vol. 114, pp. 653–658, 1992.
16. W. W. Yuen, Absorption Mean Beam Length: An Effective Length Scale for the Analysis of Radiative Heat Transfer in Absorbing, Emitting and Scattering Media, to appear in The Symposium on Thermal Science and Engineering in Honor of Chancellor Chang-Lin Tien, Nov. 1995.
17. D. K. Edwards, Molecular Gas Band Radiation, *Adv. Heat Transfer,* Vol. 12, pp. 115–193, 1976.
18. H. C. Van der Hulst, *Light Scattering By Small Particles,* John Wiley and Son, New York, 1957.
19. H. R. Phillips, Infrared Optical Properties of Graphite, *Phys. Rev. B,* Vol. 16, No. 6, p. 2896, 1977.
20. C. F. Bohrn and D. R. Huffman, *Absorption and Scattering of Light By Small Particles,* John Wiley and Son, New York, 1983.
21. Private communication with Acurex Environmental Corporation, Mountain View, California, 1995.
22. W. W. Yuen and E. E. Takara, Development of a Generalized Zonal Method for the Analysis of Radiative Transfer in Absorbing and Anisotropically Scattering Media, *Numerical Heat Transfer,* Part B, Vol. 25, 1994.

APPENDIX A. EVALUATION OF THE NORMALIZED EXCHANGE FACTORS

As shown in Section 2, four normalized exchange factors, F_{gg}, F_{gs}, F_{ssp}, and F_{sst} are sufficient to characterize the radiative exchange between cube-square elements. In Tables A.1 thru A.4, tabulated values of these exchange factors are presented. These factors are identified by the optical thickness and a three-number sequence (kD, n_x, n_y, n_z). Illustrative examples of the numbering sequence are given in Figures A.1, A.2, A.3, and A.4. The numbers on a line are tabulated in order of increasing optical thickness as shown. The first four digits in each number represent a decimal fraction. The sign and remaining digits are the power of 10 by which the fraction is to be multiplied (e.g., 8128-1 equals 0.8128×10^{-1}. All values are accurate to within a relative error of less than 1%.

Table A.1 Tabulated Values of $F_{gg}(kD, n_x, n_y, n_z)$

n_x, n_y, n_z	kD = 0.01	0.1	0.2	0.5	1.0	2.0	3.0	4.0
111	1785 1	1747 1	1698 1	1557 1	1339 1	1038 1	8401 0	7020 0
112	3956 0	3731 0	3119 0	2588 0	1813 0	9877 –1	6004 –1	3968 –1
113	8128 –1	6846 –1	5557 –1	3231 –1	1310 –1	2386 –2	4864 –3	1084 –3
114	3498 –1	2686 –1	1711 –1	8414 –2	2051 –2	1350 –3	1001 –4	8183 –6
115	1932 –1	1354 –1	9168 –2	2838 –2	4161 –3	9979 –5	2712 –6	8177 –8
122	1789 0	1602 0	1394 0	9778 –1	5588 –1	2093 –1	9217 –2	4643 –2
123	6460 –1	5325 –1	4410 –1	2286 –1	8273 –2	1213 –2	2035 –3	3825 –4
124	3139 –1	2375 –1	1688 –1	6971 –2	1568 –2	8835 –4	5665 –5	4053 –6
125	1815 –1	1258 –1	9218 –2	2510 –2	3461 –3	7359 –5	1783 –6	4883 –8
133	3960 –1	3090 –1	2347 –1	1040 –1	2788 –2	2245 –3	2099 –4	2233 –5
134	2395 –1	1740 –1	1200 –1	4272 –2	7691 –3	2794 –4	1172 –5	5595 –7
135	1535 –1	1031 –1	7377 –2	1787 –2	2069 –3	3115 –5	5409 –7	1082 –8
144	1712 –1	1174 –1	7846 –2	2233 –2	2906 –3	5552 –5	1232 –6	3158 –8
145	1220 –1	7810 –2	4635 –2	1094 –2	9719 –4	8626 –6	8905 –8	1067 –9
155	9454 –2	5703 –2	3046 –2	6134 –3	3915 –4	1796 –6	1011 –8	5978 –11
222	1127 0	9766 –1	8374 –1	5250 –1	2523 –1	6758 –2	2177 –2	8296 –3
223	5346 –1	4321 –1	3449 –1	1701 –1	5535 –2	6606 –3	9161 –4	1448 –4
224	2845 –1	2123 –1	1526 –1	5856 –2	1219 –2	5914 –4	3291 –5	2064 –6
225	1712 –1	1173 –1	8797 –2	2231 –2	2898 –3	5479 –5	1187 –6	2936 –8
233	3506 –1	2693 –1	2028 –1	8461 –2	2078 –2	1412 –3	1122 –4	1026 –5
234	2219 –1	1592 –1	1079 –1	3700 –2	6222 –3	1976 –4	7283 –6	3078 –7
235	1460 –1	9710 –2	6625 –2	1609 –2	1763 –3	2379 –5	3716 –7	6720 –9
244	1619 –1	1099 –1	7410 –2	1994 –2	2448 –3	4165 –5	8263 –7	1911 –8
245	1171 –1	7433 –2	4268 –2	1000 –2	8458 –4	6803 –6	6378 –8	6970 –10
255	9158 –2	5480 –2	2884 –2	5690 –3	3476 –4	1461 –6	7550 –9	4106 –11
333	2603 –1	1916 –1	1365 –1	4986 –2	9668 –3	4105 –4	2045 –5	1185 –6
334	1816 –1	1259 –1	8602 –2	2508 –2	3479 –3	7536 –5	1909 –6	5636 –8
335	1272 –1	8222 –2	5011 –2	1199 –2	1121 –3	1103 –5	1266 –7	1696 –9
344	1392 –1	9167 –2	5945 –2	1455 –2	1512 –3	1845 –5	2641 –7	4459 –9
345	1046 –1	6471 –2	3409 –2	7765 –3	5684 –4	3436 –6	2562 –8	2018 –10
355	8370 –2	4894 –2	2623 –2	4586 –3	2464 –4	8035 –7	3224 –9	1370 –11
444	1127 –1	7087 –2	3503 –2	9178 –3	7393 –4	5420 –6	4673 –8	4760 –10
445	8880 –2	5273 –2	2671 –2	5288 –3	3094 –4	1196 –6	5719 –9	2903 –11
455	7315 –2	4124 –2	2124 –2	3287 –3	1443 –4	3145 –7	8439 –10	2412 –12
555	6211 –2	3340 –2	1722 –2	2155 –3	7271 –5	9379 –8	1482 –10	2508 –13

If numerical evaluation is needed, three approaches are recommended. The selection of the approach depends on the optical thickness, the geometry of the considered volume (or area) elements, and the availability of previously tabulated data of normalized exchange factors. These approaches are described in detail in the following three subsections.

A.1 Direct Numerical Integration

With advanced computational equipment, this approach is quite feasible when the two volume (or area) elements are disjointed or are connected by only common edges. The convergence can be slow when the optical thickness is large. However, this method has serious difficulties for exchange factors between joined elements (with common surfaces and/or common volumes) in which the integrand has a singularity. Even with modern high-speed workstations, a "brute force" numerical integration cannot converge to acceptable degree of accuracy (say, within 1%) for elements with moderate or large optical thicknesses.

A.2 Superposition

The approach is particularly effective in building up exchange factors with large optical thickness using available data with smaller optical thicknesses. For example, if F_{gg} is known for $k_{a,ij}D = 0.1$ and $\eta_x, \eta_y, \eta_z = 1, 2, \ldots 10$, the self-self exchange factor F_{gg} (1.0, 1, 1, 1) can be obtained by

$$F_{gg}(1.0, 1, 1, 1) = (0.1)^2 \times \sum_{i_x=1}^{10}\sum_{i_y=1}^{10}\sum_{i_z=1}^{10}\sum_{i'_x=1}^{10}\sum_{i'_y=1}^{10}\sum_{i'_z=1}^{10} F_{gg}\left(0.1, \left|i_x - i'_x + 1\right|, \left|i_y - i'_y + 1\right|, \left|i_z - i'_z + 1\right|\right) \qquad (A.1)$$

If each of the normalized exchange factors with the optical thickness of 0.1 are tabulated to an accuracy of 1% relative error, the exchange factor generated by the summation also has a relative error of 1%.

A.3 Superposition and Direct Numerical Integration

With joint elements for which the exchange factor must be calculated numerically, the difficulty with the singularity can be avoided by first evaluating a basic differential exchange factor. The specific geometry is shown in Figure A.5. The differential exchange factor between dV and A is given by

$$dgs = dVM\left(kX, \frac{Y}{X}, \frac{Z}{X}\right) \qquad (A.2)$$

Table A.2 Tabulated Values of $F_{gs}(kD, n_x, n_y, n_z)$

n_x, n_y, n_z	kD = 0.01	0.1	0.2	0.5	1.0	2.0	3.0	4.0
111	6636 0	6371 0	6100 0	5411 0	4474 0	3247 0	2506 0	2025 0
112	1248 0	1097 0	9437 –1	6017 –1	2943 –1	7173 –2	1884 –2	5140 –3
113	4769 –1	3821 –1	2939 –1	1425 –1	3995 –2	3751 –3	3574 –4	3645 –5
114	2457 –1	1794 –1	1292 –1	4456 –2	7472 –3	2605 –4	9349 –6	3497 –7
115	1481 –1	9850 –2	6195 –2	1516 –2	1667 –3	2152 –5	2853 –7	3545 –9
121	1337 0	1230 0	1133 0	8801 –1	5920 –1	2997 –1	1704 –1	1068 –1
122	7862 –1	6784 –1	5669 –1	3361 –1	1479 –1	2976 –2	6480 –3	1492 –3
123	3881 –1	3072 –1	2343 –1	1071 –1	2893 –2	2246 –3	1808 –4	1629 –5
124	2194 –1	1588 –1	1135 –1	3661 –2	6250 –3	1796 –4	5765 –6	1940 –7
125	1381 –1	9155 –2	5727 –2	1410 –2	1498 –3	1629 –5	1968 –7	2222 –9
131	1907 –1	1620 –1	1346 –1	7508 –2	3046 –2	5175 –3	9440 –4	1882 –4
132	3053 –1	2472 –1	1940 –1	9521 –2	3013 –2	3156 –3	3555 –4	4584 –5
133	2349 –1	1776 –1	1298 –1	5123 –2	1099 –2	5305 –4	2776 –5	1673 –6
134	1625 –1	1141 –1	7807 –2	2367 –2	3258 –3	6369 –5	1464 –6	3571 –8
135	1135 –1	7349 –2	4530 –2	1061 –2	9268 –4	7354 –6	6738 –8	5729 –10
141	5702 –2	4402 –2	3260 –2	1388 –2	3277 –3	1854 –4	1365 –5	1085 –6
142	1251 –1	9375 –2	6618 –2	2598 –2	5260 –3	2129 –4	1117 –5	6415 –7
143	1296 –1	9225 –2	6110 –2	2032 –2	3064 –3	7038 –5	2023 –6	6365 –8
144	1088 –1	7248 –2	4463 –2	1190 –2	1246 –3	1395 –5	1889 –7	2714 –9
145	8566 –2	5297 –2	3067 –2	6301 –3	4300 –4	2179 –6	1283 –8	6930 –11
151	2388 –2	1681 –2	1223 –2	3569 –3	4884 –4	1070 –5	2898 –7	6401 –9
152	5970 –2	4111 –2	2846 –2	7850 –3	9638 –4	1628 –5	3412 –7	5988 –9
153	7305 –2	4824 –2	3108 –2	7676 –3	7594 –4	7983 –6	1039 –7	1171 –9
154	7065 –2	4409 –2	2627 –2	5491 –3	3929 –4	2275 –6	1570 –8	9650 –11
155	6185 –2	3623 –2	2024 –2	3394 –3	1693 –4	4762 –7	1570 –9	4696 –12
221	5444 –1	4854 –1	4268 –1	2953 –1	1656 –1	5888 –2	2434 –2	1157 –2
222	5411 –1	4568 –1	3709 –1	2066 –1	8154 –2	1331 –2	2397 –3	4675 –4
223	3228 –1	2519 –1	1891 –1	8224 –2	2064 –2	1356 –3	9475 –5	7529 –6
224	1973 –1	1415 –1	9972 –2	3196 –2	5031 –3	1256 –4	3610 –6	1093 –7
225	1291 –1	8499 –2	5285 –2	1300 –2	1290 –3	1242 –5	1368 –7	1405 –9
231	1380 –1	1146 –1	9248 –2	4876 –2	1770 –2	2425 –3	3707 –4	6355 –5
232	2445 –1	1948 –1	1489 –1	6984 –2	2005 –2	1747 –3	1682 –4	1876 –5
233	2046 –1	1526 –1	1091 –1	4153 –2	8282 –3	3472 –4	1593 –5	8508 –7
234	1487 –1	1032 –1	6903 –2	2034 –2	2656 –3	4620 –5	9555 –7	2104 –8
235	1069 –1	6851 –2	4179 –2	9502 –3	7879 –4	5710 –6	4786 –8	3717 –10
241	4867 –2	3703 –2	2677 –2	1106 –2	2356 –3	1164 –4	7448 –6	5207 –7
242	1099 –1	8123 –2	5619 –2	2127 –2	3991 –3	1410 –4	6495 –6	3299 –7
243	1177 –1	8283 –2	5402 –2	1735 –2	2452 –3	5011 –5	1285 –6	3630 –8
244	1014 –1	6697 –2	4051 –2	1055 –2	1043 –3	1058 –5	1300 –7	1698 –9
245	8141 –2	4992 –2	2851 –2	5737 –3	3719 –4	1735 –6	9392 –9	4662 –11
251	2179 –2	1518 –2	1078 –2	3050 –3	3950 –4	7692 –6	1861 –7	3695 –9
252	5502 –2	3747 –2	2542 –2	6855 –3	7872 –4	1197 –5	2253 –7	3568 –9
253	6830 –2	4469 –2	2833 –2	6828 –3	6312 –4	6081 –6	7178 –8	7356 –10
254	6702 –2	4146 –2	2445 –2	4986 –3	3401 –4	1799 –6	1138 –8	6414 –11
255	5936 –2	3452 –2	1914 –2	3122 –3	1499 –4	3889 –7	1187 –9	3287 –12
331	6820 –2	5358 –2	4073 –2	1829 –2	4756 –3	3651 –4	3121 –5	3194 –6
332	1446 –1	1097 –1	7976 –2	3222 –2	7150 –3	3739 –4	2202 –5	1560 –6
333	1438 –1	1034 –1	7066 –2	2379 –2	3860 –3	1087 –4	3377 –6	1246 –7
334	1170 –1	7870 –2	5001 –2	1350 –2	1494 –3	1865 –5	2821 –7	4579 –9
335	9031 –2	5629 –2	3347 –2	6950 –3	4972 –4	2757 –6	1776 –8	1055 –10
341	3269 –2	2390 –2	1642 –2	5968 –3	1006 –3	3302 –5	1389 –6	6513 –8
342	7864 –2	5607 –2	3708 –2	1248 –2	1877 –3	4548 –5	1424 –6	4984 –8
343	9108 –2	6199 –2	3881 –2	1124 –2	1327 –3	1931 –5	3545 –7	7238 –9
344	8380 –2	5374 –2	3129 –2	7504 –3	6285 –4	4798 –6	4428 –8	4364 –10
345	7056 -2	4228 –2	2340 –2	4380 –3	2480 –4	8959 –7	3788 –9	1465 –11

Table A.2 Tabulated Values of $F_{gs}(kD, n_x, n_y, n_z)$ (continued)

n_x, n_y, n_z	kD = 0.01	0.1	0.2	0.5	1.0	2.0	3.0	4.0
351	1699 –2	1147 –2	7697 –3	2018 –3	2190 –4	3032 –6	5269 –8	7617 –10
352	4405 –2	2915 –2	1877 –2	4661 –3	4541 –4	5009 –6	6880 –8	8024 –10
353	5670 –2	3609 –2	2203 –2	4873 –3	3869 –4	2792 –6	2472 –8	1909 –10
354	5774 –2	3491 –2	2007 –2	3772 –3	2246 –4	9122 –7	4464 –9	1949 –11
355	5274 –2	2999 –2	1623 –2	2459 –3	1051 –4	2156 –7	5243 –10	1155 –12
441	1994 –2	1375 –2	8624 –3	2648 –3	3235 –4	5677 –6	1264 –7	3139 –9
442	5084 –2	3428 –2	2081 –2	5995 –3	6552 –4	8995 –6	1558 –7	3009 –9
443	6408 –2	4152 –2	2394 –2	6077 –3	5362 –4	4700 –6	5114 –8	6172 –10
444	6380 –2	3917 –2	2161 –2	4533 –3	2956 –4	1435 –6	8405 –9	5219 –11
445	5710 –2	3295 –2	1730 –2	2878 –3	1330 –4	3194 –7	9083 –10	2352 –12
451	1209 –2	7784 –3	4752 –3	1016 –3	9252 –5	7586 –7	7847 –9	6838 –11
452	3221 –2	2035 –2	1209 –2	2669 –3	2019 –4	1349 –6	1130 –8	8095 –11
453	4348 –2	2652 –2	1512 –2	2980 –3	1868 –4	8491 –7	4769 –9	2342 –11
454	4633 –2	2698 –2	1460 –2	2452 –3	1186 –4	3171 –7	1030 –9	2984 –12
455	4408 –2	2425 –2	1243 –2	1695 –3	6037 –5	8505 –8	1432 –10	2184 –13
551	8210 –3	4924 –3	2982 –3	5080 –4	3310 –5	1407 –7	7539 –10	3434 –12
552	2266 –2	1351 –2	7834 –3	1376 –3	7582 –5	2690 –7	1196 –9	4574 –12
553	3181 –2	1838 –2	1027 –2	1628 –3	7603 –5	1910 –7	5953 –10	1622 –12
554	3561 –2	1969 –2	1036 –2	1427 –3	5301 –5	8221 –8	1559 –10	2630 –13
555	3549 –2	1858 –2	9219 –3	1061 –3	2954 –5	2536 –8	2623 –11	2448 –14

where

$$M\left(kX, \frac{Y}{X}, \frac{Z}{X}\right) = \frac{1}{\pi}\int_A \frac{(\vec{n}_1 \cdot \vec{\eta}_r)e^{-k\gamma\eta_r}}{\eta_r^3} d\eta_y d\eta_z \tag{A.3}$$

Using the angular coordinate as defined in Figure A.5 and some algebraic manipulation, the integral can be reduced to

$$M\left(kX, \frac{Y}{X}, \frac{Z}{X}\right) = \frac{E_2(kX)}{2} - \frac{1}{\pi}\int_0^{\frac{\pi}{2}} \left[R_u^2 + 1\right]^{-\frac{1}{2}} E_2\left[kX\left(R_u^2 + 1\right)^{\frac{1}{2}}\right] d\phi \tag{A.4}$$

where

$$R_u = \begin{cases} \dfrac{Y}{X\cos\phi} & 0 \le \phi \tan^{-1}\dfrac{Z}{Y} \\ \dfrac{Z}{X\sin\phi} & \tan^{-1}\dfrac{Z}{Y} \le \phi \le \dfrac{\pi}{2} \end{cases} \tag{A.5}$$

and $E_2(x)$ is the exponential integral function defined by

$$E_2(x) = \int_1^\infty \frac{1}{t^2} e^{-xt} dt \tag{A.6}$$

Table A.3 Tabulated Values of $F_{ssp}(kD, n_x, n_y, n_z)$

n_x n_y n_z	kD =0	0.01	0.1	0.2	0.5	1.0	2.0	3.0	4.0
111	1998 0	1976 0	1789 0	1570 0	1148 0	6618 –1	2210 –1	7435 –2	2518 –2
112	6862 –1	6721 –1	5577 –1	4445 –1	2435 –1	8648 –2	1094 –2	1388 –3	1768 –4
113	3298 –1	3198 –1	2430 –1	1753 –1	7171 –2	1560 –2	7395 –4	3509 –5	1668 –6
114	1911 –1	1836 –1	1276 –1	8312 –2	2535 –2	3364 –3	5930 –5	1046 –6	1857 –8
115	1240 –1	1180 –1	7502 –2	4248 –2	1002 –2	8094 –4	5285 –6	3465 –8	2267 –10
121	8606 –1	8492 –1	7538 –1	6585 –1	4462 –1	2341 –1	6643 –2	1949 –2	5874 –3
122	4807 –1	4700 –1	3839 –1	3038 –1	1566 –1	5134 –2	5615 –3	6267 –4	7119 –5
123	2736 –1	2650 –1	1989 –1	1428 –1	5559 –2	1133 –2	4764 –4	2027 –5	8724 –7
124	1708 –1	1638 –1	1127 –1	7337 –2	2144 –2	2698 –3	4303 –5	6921 –7	1124 –8
125	1151 –1	1094 –1	6897 –2	3090 –2	8886 –3	6864 –4	4118 –6	2490 –8	1511 –10
131	1527 –1	1496 –1	1244 –1	1-43 –1	5548 –2	2069 –2	3081 –3	4943 –4	8407 –5
132	2060 –1	2003 –1	1563 –1	1193 –1	5220 –2	1345 –2	9363 –4	6873 –5	5276 –6
133	1686 –1	1626 –1	1177 –1	8247 –2	2814 –2	4752 –3	1397 –4	4267 –6	1345 –7
134	1256 –1	1201 –1	8030 –2	5133 –2	1344 –2	1450 –3	1722 –5	2101 –7	2612 –9
135	9337 –2	8847 –2	5443 –2	3107 –2	6302 –3	4275 –4	1998 –6	9511 –9	4605 –11
141	3569 –2	3463 –2	2645 –2	1997 –2	8094 –3	1896 –3	1135 –4	7485 –6	5319 –7
142	7946 –2	7672 –2	5596 –2	3923 –2	1391 –2	2499 –3	8633 –5	3229 –6	1288 –7
143	8993 –2	8623 –2	5913 –2	3808 –2	1114 –2	1406 –3	2359 –5	4207 –7	7733 –9
144	8160 –2	7764 –2	4960 –2	2920 –2	6809 –3	5762 –4	4288 –6	3317 –8	2681 –10
145	6856 –2	6468 –2	3829 –2	2135 –2	3741 –3	2063 –4	6465 –7	2088 –9	6982 –12
151	1183 –2	1137 –2	7947 –3	6039 –3	1638 –3	2351 –4	5326 –6	1344 –7	3478 –9
152	3333 –2	3191 –2	2153 –2	1517 –2	3796 –3	4459 –4	6678 –6	1100 –7	1872 –9
153	4693 –2	4466 –2	2865 –2	1842 –2	4023 –3	3533 –4	2918 –6	2558 –8	2417 –10
154	5021 –2	4746 –2	2863 –2	1667 –2	3051 –3	1891 –4	7665 –7	3270 –9	1483 –11
155	4745 –2	4451 –2	2506 –2	1370 –2	1964 –3	8261 –5	1524 –7	2939 –10	5954 –13
221	4331 –1	4264 –1	3707 –1	3180 –1	2007 –1	9500 –2	2245 –2	5646 –3	1492 –3
222	3511 –1	3427 –1	2756 –1	2147 –1	1051 –1	3179 –2	3002 –3	2940 –4	2972 –5
223	2302 –1	2227 –1	1651 –1	1175 –1	4376 –2	8373 –3	3123 –4	1191 –5	4639 –7
224	1534 –1	1470 –1	1002 –1	6488 –2	1825 –2	2180 –3	3150 –5	4619 –7	6870 –9
225	1071 –1	1016 –1	6358 –2	3605 –2	7901 –3	5844 –4	3224 –6	1799 –8	1013 –10
231	1051 –1	1028 –1	8396 –2	6826 –2	3454 –2	1170 –2	1459 –3	2002 –4	2969 –5
232	1644 –1	1597 –1	1228 –1	9200 –2	3855 –2	9221 –3	5577 –4	3602 –5	2463 –6
233	1464 –1	1410 –1	1009 –1	6955 –2	2297 –2	3653 –3	9588 –5	2633 –6	7437 –8
234	1144 –1	1093 –1	7239 –2	4558 –2	1163 –2	1193 –3	1289 –5	1438 –7	1641 –9
235	8745 –2	8279 –2	5054 –2	2886 –2	5651 –3	3675 –4	1583 –6	6971 –9	3137 –11
241	2929 –2	2838 –2	2137 –2	1568 –2	6148 –3	1335 –3	6928 –5	4002 –6	2522 –7
242	6853 –2	6607 –2	4762 –2	3266 –2	1123 –2	1891 –3	5777 –5	1926 –6	6648 –8
243	8088 –2	7747 –2	5258 –2	3342 –2	9478 –3	1133 –3	1713 –5	2769 –7	4635 –9
244	7558 –2	7184 –2	4550 –2	2644 –2	6016 –3	4861 –4	3309 –6	2350 –8	1753 –10
245	6478 –2	6106 –2	3588 –2	1991 –2	3393 –3	1798 –4	5215 –7	1564 –9	4872 –12
251	1052 –2	1010 –2	6980 –3	5157 –3	1371 –3	1853 –4	3741 –6	8158 –8	1980 –9
252	3020 –2	2888 –2	1929 –2	1325 –2	3256 –3	3623 –4	4887 –6	7087 –8	1129 –9
253	4340 –2	4127 –2	2623 –2	1657 –2	3544 –3	2967 –4	2234 –6	1792 –8	1556 –10
254	4724 –2	4463 –2	2671 –2	1550 –2	2751 –3	1634 –4	6107 –7	2408 –9	1013 –11
255	4524 –2	4241 –2	2371 –2	1283 –2	1804 –3	7309 –5	1255 –7	2256 –10	4275 –13
331	4481 –2	4356 –2	3381 –2	2596 –2	1112 –2	2861 –3	2095 –4	1729 –5	1580 –6
332	9341 –2	9032 –2	6673 –2	4793 –2	1756 –2	3389 –3	1356 –4	5936 –6	2805 –7
333	1006 –1	9659 –2	6693 –2	4448 –2	1320 –2	1764 –3	3318 –5	6647 –7	1382 –8
334	8838 –2	8417 –2	5424 –2	3284 –2	7740 –3	6867 –4	5612 –6	4769 –8	4237 –10
335	7268 –2	6862 –2	4093 –2	2347 –2	4134 –3	2374 –4	8055 –7	2816 –9	1017 –11
341	1774 –2	1711 –2	1239 –2	8615 –3	2998 –3	5259 –4	1799 –5	6984 –7	2839 –8
342	4636 –2	4453 –2	3102 –2	2042 –2	6295 –3	8816 –4	1882 –5	4460 –7	1107 –8
343	6054 –2	5780 –2	3811 –2	2334 –2	6044 –3	6173 –4	6885 –6	8178 –8	1051 –9
344	6099 –2	5781 –2	3571 –2	2022 –2	4230 –3	2987 –4	1566 –6	8640 –9	5066 –11
345	5512 –2	5183 –2	2980 –2	1610 –2	2562 –3	1207 –4	2789 –7	6712 –10	1693 –12

Table A.3 Tabulated Values of $F_{ssp}(kD, n_x, n_y, n_z)$ (continued)

n_x n_y n_z	kD =0	0.01	0.1	0.2	0.5	1.0	2.0	3.0	4.0
351	7667 –3	7332 –3	4911 –3	3399 –3	8402 –4	9574 –5	1382 –6	2186 –8	3906 –10
352	2305 –2	2197 –2	1426 –2	9334 –3	2121 –3	2019 –4	2007 –6	2169 –8	2610 –10
353	3489 –2	3308 –2	2050 –2	1248 –2	2474 –3	1803 –4	1035 –6	6389 –9	4316 –11
354	3976 –2	3746 –2	2192 –2	1252 –2	2043 –3	1073 –4	3156 –7	9864 –10	3321 –12
355	3947 –2	3692 –2	2023 –2	1056 –2	1408 –3	5117 –5	7063 –8	1038 –10	1612 –13
441	9428 –3	9037 –3	6180 –3	3902 –3	1159 –3	1484 –4	2716 –6	5484 –8	1263 –9
442	2750 –2	2627 –2	1738 –2	1049 –2	2813 –3	2975 –4	3655 –6	4904 –8	7368 –10
443	4026 –2	3824 –2	2411 –2	1373 –2	3136 –3	2508 –4	1733 –6	1289 –8	1052 –10
444	4453 –2	4204 –2	2497 –2	1361 –2	2486 –3	1418 –4	4903 –7	1801 –9	7132–12
445	4319 –2	4046 –2	2247 –2	1127 –2	1659 –3	6482 –5	1038 –7	1748 –10	3124 –13
451	4947 –3	4707 –3	3006 –3	1880 –3	4168 –4	3655 –5	3142 –7	2991 –9	3249 –11
452	1570 –2	1489 –2	9257 –3	5541 –3	1132 –3	8459 –5	5214 –7	3529 –9	2688 –11
453	2536 –2	2394 –2	1426 –2	8109 –3	1442 –3	8444 –5	3154 –7	1278 –9	5737 –12
454	3069 –2	2880 –2	1626 –2	8721 –3	1294 –3	5588 –5	1118 –7	2402 –10	5620 –13
455	3202 –2	2984 –2	1584 –2	7875 –3	9566 –4	2916 –5	2852 –8	2999 –11	3364 –14
551	3039 –3	2872 –3	1730 –3	1055 –3	1844 –4	1165 –5	5119 –8	2594 –10	1478 –12
552	1013 –2	9550 –3	5611 –3	3303 –3	5361 –4	2942 –5	9682 –8	3630 –10	1517 –12
553	1741 –2	1634 –2	9245 –3	5166 –3	7444 –4	3283 –5	6919 –8	1634 –10	4254 –13
554	2240 –2	2091 –2	1126 –2	5886 –3	7284 –4	2431 –5	2904 –8	3822 –11	5477 –14
555	2467 –2	2288 –2	1164 –2	5669 –3	5822 –4	1405 –5	8681 –9	5821 –12	4200 –15

Note that the integrand in Eq. (A.4) is free of singularity and can be readily evaluated numerically.

For the evaluation of $F_{gs}(kD, 1, 1, 1)$ and $F_{gs}(kD, 1, 1, 2)$ as defined by Eq. (10), super-position can be used to yield

$$F_{gs}(kD, 1, 1, 1) = \frac{1}{\pi}\int_0^1\int_0^1\int_0^1 N_1\left(kD, \eta_x, \eta_y, \eta_z\right)d\eta_x d\eta_y d\eta_z \qquad (A.7)$$

with

$$\begin{aligned} N_1\left(kD, \eta_x, \eta_y, \eta_z\right) = {} & M\left[kD(1-\eta_z), \frac{\eta_y}{1-\eta_z}, \frac{\eta_x}{1-\eta_z}\right] \\ & + M\left[kD(1-\eta_z), \frac{1-\eta_y}{1-\eta_z}, \frac{\eta_x}{1-\eta_z}\right] \\ & + M\left[kD(1-\eta_z), \frac{\eta_y}{1-\eta_z}, \frac{1-\eta_x}{1-\eta_z}\right] \\ & + M\left[kD(1-\eta_z), \frac{1-\eta_y}{1-\eta_z}, \frac{1-\eta_x}{1-\eta_z}\right] \end{aligned} \qquad (A.8)$$

and

Table A.4 Tabulated Values of $F_{sst}(kD, n_x, n_y, n_z)$

n_x n_y n_z	kD =0	0.01	0.1	0.2	0.5	1.0	2.0	3.0	4.0
111	2000 0	1989 0	1893 0	1799 0	1539 0	1218 0	8280 –1	6107 –1	4787 –1
112	3280 –1	3229 –1	2804 –1	2366 –1	1509 –1	7072 –2	1631 –2	3984 –3	1021 –3
113	8904 –2	8681 –2	6909 –2	5328 –2	2525 –2	7293 –3	6398 –4	5940 –5	5777 –6
114	3466 –2	3346 –2	2437 –2	1709 –2	6002 –3	1059 –3	3475 –5	1210 –6	4356 –8
115	1675 –2	1601 –2	1066 –2	6767 –3	1766 –3	1898 –4	2312 –6	2899 –8	4016 –10
121	3281 –1	3229 –1	2804 –1	2366 –1	1509 –1	7072 –2	1631 –2	3984 –3	1021 –3
122	3294 –1	3226 –1	2672 –1	2177 –1	1166 –1	4216 –2	5859 –3	8783 –4	1404 –4
123	1588 –1	1543 –1	1188 –1	8839 –2	3762 –2	9093 –3	5632 –4	3744 –5	2644 –6
124	7763 –2	7474 –2	5312 –2	3617 –2	1174 –2	1812 –3	4566 –5	1230 –6	3469 –8
125	4180 –2	3986 –2	2604 –2	1602 –2	3957 –3	3820 –4	3766 –6	3855 –8	4360 –10
131	8903 –2	8680 –2	6909 –2	5328 –2	2525 –2	7293 –3	6397 –4	5940 –5	5777 –6
132	1588 –1	1543 –1	1188 –1	8839 –2	3762 –2	9094 –3	5632 –4	3744 –5	2645 –6
133	1240 –1	1197 –1	8726 –2	6167 –2	2153 –2	3815 –3	1273 –4	4582 –6	1757 –7
134	7995 –2	7659 –2	5207 –2	3383 –2	9449 –3	1140 –3	1762 –5	2931 –7	5157 –9
135	5035 –2	4783 –2	3013 –2	1766 –2	3894 –3	3073 –4	2030 –6	1407 –8	1075 –10
141	3466 –2	3346 –2	2437 –2	1709 –2	6002 –3	1059 –3	3475 –5	1210 –6	4430 –8
142	7763 –2	7474 –2	5312 –2	3617 –2	1174 –2	1812 –3	4566 –5	1230 –6	3511 –8
143	7995 –2	7659 –2	5207 –2	3383 –2	9450 –3	1140 –3	1762 –5	2930 –7	5186 –9
144	6410 –2	6101 –2	3912 –2	2385 –2	5474 –3	4773 –4	3858 –6	3319 –8	3109 –10
145	4699 –2	4439 –2	2660 –2	1503 –2	2754 –3	1649 –4	6275 –7	2529 –9	1116 –11
151	1675 –2	1601 –2	1066 –2	6767 –3	1766 –3	1898 –4	2311 –6	3017 –8	4078 –10
152	4180 –2	3986 –2	2604 –2	1602 –2	3957 –3	3820 –4	3766 –6	3982 –8	4415 –10
153	5035 –2	4783 –2	3013 –2	1766 –2	3894 –3	3074 –4	2030 –6	1437 –8	1084 –10
154	4699 –2	4439 –2	2660 –2	1503 –2	2754 –3	1648 –4	6275 –7	2552 –9	1121 –11
155	3899 –2	3659 –2	2065 –2	1117 –2	1639 –3	7042 –5	1380 –7	2882 –10	6551 –13
211	4058 –1	4018 –1	3678 –1	3414 –1	2518 –1	1624 –1	7566 –2	4035 –2	2410 –2
212	1892 –1	1858 –1	1581 –1	1308 –1	7788 –2	3284 –2	6264 –3	1297 –3	2884 –4
213	6862 –2	6679 –2	5236 –2	3959 –2	1790 –2	4774 –3	3608 –4	2928 –5	2522 –6
214	2994 –2	2887 –2	2078 –2	1435 –2	4861 –3	8060 –4	2346 –5	7315 –7	2378 –8
215	1527 –2	1458 –2	9624 –3	6016 –3	1528 –3	1561 –4	1724 –6	1970 –8	2503 –10
221	1892 –1	1858 –1	1581 –1	1308 –1	7787 –2	3284 –2	6264 –3	1297 –3	2884 –4
222	2304 –1	2252 –1	1832 –1	1455 –1	7402 –2	2438 –2	2851 –3	3656 –4	5088 –5
223	1290 –1	1252 –1	9513 –2	6947 –2	2833 –2	6362 –3	3427 –4	2003 –5	1256 –6
224	6833 –2	6570 –2	4618 –2	3096 –2	9726 –3	1414 –3	3181 –5	7706 –7	1967 –8
225	3841 –2	3660 –2	2369 –2	1435 –2	3459 –3	3179 –4	2851 –6	2668 –8	2771 –10
231	6863 –2	6679 –2	5236 –2	3959 –2	1790 –2	4774 –3	3607 –4	2928 –5	2523 –6
232	1290 –1	1252 –1	9513 –2	6947 –2	2833 –2	6362 –3	3427 –4	2003 –5	1257 –6
233	1071 –1	1033 –1	7437 –2	5162 –2	1742 –2	2898 –3	8569 –5	2750 –6	9464 –8
234	7221 –2	6910 –2	4651 –2	2976 –2	8080 –3	9242 –4	1288 –5	1942 –7	3114 –9
235	4684 –2	4445 –2	2777 –2	1612 –2	3458 –3	2607 –4	1576 –6	1004 –8	7079 –11
241	2994 –2	2887 –2	2078 –2	1435 –2	4861 –3	8061 –4	2346 –5	7315 –7	2415 –8
242	6833 –2	6570 –2	4618 –2	3096 –2	9726 –3	1414 –3	3181 –5	7706 –7	1990 –8
243	7221 –2	6910 –2	4651 –2	2976 –2	8080 –3	9242 –4	1288 –5	1942 –7	3131 –9
244	5929 –2	5638 –2	3585 –2	2155 –2	4825 –3	4013 –4	2958 –6	2329 –8	2008 –10
245	4427 –2	4179 –2	2485 –2	1395 –2	2488 –3	1428 –4	5013 –7	1868 –9	7659 –12
251	1527 –2	1458 –2	9624 –3	6016 –3	1528 –3	1561 –4	1724 –6	2047 –8	2540 –10
252	3841 –2	3660 –2	2369 –2	1435 –2	3459 –3	3180 –4	2851 –6	2751 –8	2805 –10
253	4684 –2	4445 –2	2776 –2	1612 –2	3458 –3	2607 –4	1576 –6	1024 –8	7136 –11
254	4427 –2	4179 –2	2485 –2	1395 –2	2488 –3	1428 –4	5013 –7	1885 –9	7687 –12
255	3716 –2	3485 –2	1953 –2	1046 –2	1504 –3	6224 –5	1133 –7	2203 –10	4678 –13
311	4312 –2	4228 –2	3543 –2	2995 –2	1636 –2	6411 –3	1070 –3	1968 –4	3919 –5
312	5859 –2	5717 –2	4589 –2	3637 –2	1750 –2	5396 –3	5603 –4	6470 –5	8188 –6
313	3618 –2	3505 –2	2632 –2	1912 –2	7461 –3	1582 –3	7692 –5	4115 –6	2378 –7
314	2033 –2	1952 –2	1359 –2	9010 –3	2744 –3	3798 –4	7808 –6	1749 –7	4160 –9
315	1184 –2	1127 –2	7237 –3	4354 –3	1019 –3	8975 –5	7437 –7	6465 –9	6324 –11

Table A.4 Tabulated Values of $F_{sst}(kD, n_x, n_y, n_z)$ (continued)

n_x n_y n_z	kD =0	0.01	0.1	0.2	0.5	1.0	2.0	3.0	4.0
321	5860 –2	5718 –2	4590 –2	3637 –2	1750 –2	5395 –3	5603 –4	6470 –5	8188 –6
322	1005 –1	9773 –2	7572 –2	5725 –2	2466 –2	6235 –3	4356 –4	3399 –5	2928 –6
323	7627 –2	7365 –2	5382 –2	3782 –2	1350 –2	2457 –3	8810 –5	3490 –6	1503 –7
324	4850 –2	4647 –2	3165 –2	2051 –2	5799 –3	7107 –4	1147 –5	2026 –7	3828 –9
325	3038 –2	2886 –2	1820 –2	1067 –2	2365 –3	1885 –4	1281 –6	9189 –9	7405 –11
331	3618 –2	3504 –2	2632 –2	1912 –2	7461 –3	1582 –3	7691 –5	4115 –6	2388 –7
332	7627 –2	7365 –2	5383 –2	3782 –2	1350 –2	2457 –3	8809 –5	3491 –6	1509 –7
333	7269 –2	6982 –2	4860 –2	3245 –2	9817 –3	1361 –3	2828 –5	6466 –7	1606 –8
334	5463 –2	5211 –2	3409 –2	2102 –2	5220 –3	5112 –4	5269 –6	5822 –8	7218 –10
335	3823 –2	3618 –2	2206 –2	1263 –2	2465 –3	1627 –4	7585 –7	3760 –9	2085 –11
341	2032 –2	1952 –2	1359 –2	9010 –3	2744 –3	3798 –4	7808 –6	1749 –7	4215 –9
342	4850 –2	4648 –2	3165 –2	2051 –2	5800 –3	7109 –4	1147 –5	2026 –7	3865 –9
343	5463 –2	5211 –2	3409 –2	2102 –2	5222 –3	5112 –4	5269 –6	5888 –8	7251 –10
344	4770 –2	4523 –2	2803 –2	1639 –2	3373 –3	2444 –4	1377 –6	8349 –9	5614 –11
345	3740 –2	3521 –2	2047 –2	1126 –2	1857 –3	9441 –5	2609 –7	7715 –10	2533 –12
351	1184 –2	1127 –2	7237 –3	4354 –3	1019 –3	8975 –5	7436 –7	6684 –9	6406 –11
352	3038 –2	2886 –2	1820 –2	1067 –2	2365 –3	1885 –4	1281 –6	9444 –9	7486 –11
353	3823 –2	3619 –2	2205 –2	1263 –2	2465 –3	1627 –4	7585 –7	3828 –9	2100 –11
354	3740 –2	3521 –2	2047 –2	1126 –2	1857 –3	9441 –5	2609 –7	7778 –10	2542 –12
355	3238 –2	3029 –2	1664 –2	8686 –3	1172 –3	4341 –5	6329 –8	1001 –10	1737 –13
411	9335 –3	9063 –3	6946 –3	5284 –3	2160 –3	5179 –4	3264 –5	2285 –6	1731 –7
412	1870 –2	1809 –2	1346 –2	9625 –3	3661 –3	7420 –4	3348 –5	1690 –6	9294 –8
413	1680 –2	1616 –2	1141 –2	7646 –3	2462 –3	3726 –4	9328 –6	2605 –7	7887 –9
414	1209 –2	1154 –2	7641 –3	4788 –3	1233 –3	1294 –4	1549 –6	1985 –8	2927 –10
415	8220 –3	7787 –3	4791 –3	2699 –3	5590 –4	3904 –5	2054 –7	1150 –9	7343 –12
421	1870 –2	1809 –2	1346 –2	9625 –3	3661 –3	7419 –4	3348 –5	1690 –6	9318 –8
422	4020 –2	3878 –2	2807 –2	1930 –2	6770 –3	1178 –3	3925 –5	1467 –6	6000 –8
423	3935 –2	3776 –2	2605 –2	1689 –2	5073 –3	6748 –4	1305 –5	2820 –7	6650 –9
424	3031 –2	2889 –2	1875 –2	1120 –2	2776 –3	2614 –4	2519 –6	2615 –8	3111 –10
425	2161 –2	2044 –2	1237 –2	6924 –3	1341 –3	8543 –5	3741 –7	1751 –9	9322 –12
431	1680 –2	1616 –2	1142 –2	7646 –3	2462 –3	3726 –4	9329 –6	2605 –7	7946 –9
432	3935 –2	3776 –2	2605 –2	1689 –2	5073 –3	6747 –4	1305 –5	2820 –7	6679 –9
433	4319 –2	4125 –2	2729 –2	1678 –2	4406 –3	4631 –4	5574 –6	7324 –8	1096 –9
434	3681 –2	3494 –2	2187 –2	1254 –2	2754 –3	2118 –4	1358 –6	9436 –9	7453 –11
435	2834 –2	2671 –2	1566 –2	8592 –3	1477 –3	7894 –5	2434 –7	8062 –10	3022 –12
441	1209 –2	1154 –2	7641 –3	4788 –3	1233 –3	1294 –4	1549 –6	2035 –8	2956 –10
442	3031 –2	2889 –2	1875 –2	1120 –2	2776 –3	2614 –4	2519 –6	2663 –8	3134 –10
443	3682 –2	3495 –2	2187 –2	1254 –2	2753 –3	2118 –4	1359 –6	9522 –9	7480 –11
444	3468 –2	3273 –2	1949 –2	1076 –2	1968 –3	1148 –4	4219 –7	1683 –9	7550 –12
445	2903 –2	2722 –2	1527 –2	7883 –3	1184 –3	4957 –5	9272 –8	1903 –10	4352 –13
451	8220 –3	7787 –3	4791 –3	2699 –3	5590 –4	3904 –5	2053 –7	1182 –9	7423 –12
452	2161 –2	2044 –2	1237 –2	6924 –3	1341 –3	8544 –5	3741 –7	1791 –9	9407 –12
453	2834 –2	2671 –2	1566 –2	8592 –3	1477 –3	7894 –5	2434 –7	8186 –10	3041 –12
454	2903 –2	2722 –2	1527 –2	7883 –3	1184 –3	4956 –5	9307 –8	1917 –10	4365 –13
455	2623 –2	2445 –2	1300 –2	6396 –3	7936 –4	2462 –5	2530 –8	2846 –11	3543 –14
511	3029 –3	2911 –3	2039 –3	1574 –3	4249 –4	6186 –5	1446 –6	3659 –8	1066 –9
512	7164 –3	6868 –3	4702 –3	3363 –3	8855 –4	1134 –4	2055 –6	4046 –8	9231 –10
513	7984 –3	7619 –3	5003 –3	3401 –3	7826 –4	7939 –5	8990 –7	1106 –8	1581 –10
514	6810 –3	6554 –3	4073 –3	2503 –3	4980 –4	3705 –5	2245 –7	1472 –9	1118 –11
515	5390 –3	5076 –3	2957 –3	1711 –3	2713 –4	1406 –5	4048 –8	1293 –10	4679 –13
521	7164 –3	6868 –3	4702 –3	3363 –3	8855 –4	1134 –4	2055 –6	4067 –8	9249 –10
522	1739 –2	1663 –2	1114 –2	7706 –3	1908 –3	2168 –4	3090 –6	4816 –8	8673 –10
523	2013 –2	1917 –2	1235 –2	7926 –3	1773 –3	1614 –4	1473 –6	1467 –8	1692 –10
524	1807 –2	1711 –2	1045 –2	6175 –3	1185 –3	8019 –5	4017 –7	2185 –9	1372 –11
525	1452 –2	1365 –2	7839 –3	4404 –3	6728 –4	3207 –5	7828 –8	2119 –10	6494 –13

Table A.4 Tabulated Values of $F_{sst}(kD, n_x, n_y, n_z)$ (continued)

n_x n_y n_z	kD =0	0.01	0.1	0.2	0.5	1.0	2.0	3.0	4.0
531	7984 –3	7619 –3	5002 –3	3401 –3	7825 –4	7939 –5	8990 –7	1119 –8	1589 –10
532	2013 –2	1916 –2	1234 –2	7926 –3	1773 –3	1614 –4	1473 –6	1477 –8	1697 –10
533	2467 –2	2340 –2	1454 –2	8823 –3	1779 –3	1324 –4	8046 –7	5361 –9	4101 –11
534	2348 –2	2214 –2	1310 –2	7517 –3	1287 –3	7276 –5	2537 –7	9645 –10	4207 –12
535	1984 –2	1859 –2	1037 –2	5608 –3	7837 –4	3185 –5	5648 –8	1111 –10	2467 –13
541	6911 –3	6555 –3	4073 –3	2503 –3	4980 –4	3705 –5	2245 –7	1498 –9	1125 –11
542	1807 –2	1711 –2	1045 –2	6175 –3	1185 –3	8019 –5	4017 –7	2215 –9	1380 –11
543	2348 –2	2215 –2	1310 –2	7517 –3	1287 –3	7276 –5	2537 –7	9714 –10	4218 –12
544	2380 –2	2234 –2	1263 –2	6861 –3	1017 –3	4475 –5	9344 –8	2169 –10	5670 –13
545	2131 –2	1988 –2	1065 –2	5391 –3	6719 –4	2179 –5	2460 –8	3075 –11	4319 –14
551	5390 –3	5075 –3	2957 –3	1711 –3	2713 –4	1405 –5	4094 –8	1321 –10	4719 –13
552	1452 –2	1365 –2	7840 –3	4404 –3	6728 –4	3207 –5	7903 –8	2158 –10	6542 –13
553	1984 –2	1859 –2	1037 –2	5608 –3	7836 –4	3185 –5	5685 –8	1124 –10	2479 –13
554	2131 –2	1988 –2	1065 –2	5391 –3	6719 –4	2179 –5	2468 –8	3093 –11	4329 –14
555	2017 –2	1871 –2	9536 –3	4570 –3	4814 –4	1180 –5	7614 –9	5420 –12	4309 –15

$$F_{gs}(kD, 2, 1, 1) = \frac{1}{\pi}\int_0^1\int_0^1\int_0^1 N_2(kD, \eta_x, \eta_y, \eta_z)\,d\eta_x d\eta_y d\eta_z \qquad (A.9)$$

with

$$\begin{aligned} N_2(kD, \eta_x, \eta_y, \eta_z) = {} & M\left[kD(1-\eta_z), \frac{\eta_y}{1-\eta_z}, \frac{2-\eta_x}{1-\eta_z}\right] \\ & + M\left[kD(1-\eta_z), \frac{1-\eta_y}{1-\eta_z}, \frac{2-\eta_x}{1-\eta_z}\right] \\ & - M\left[kD(1-\eta_z), \frac{\eta_y}{1-\eta_z}, \frac{1-\eta_x}{1-\eta_z}\right] \\ & - M\left[kD(1-\eta_z), \frac{1-\eta_y}{1-\eta_z}, \frac{1-\eta_x}{1-\eta_z}\right] \end{aligned} \qquad (A.10)$$

The integrand of Eq. (A.7) is free of singularity and $F_{gs}(kD, 1, 1, 1)$ and $F_{gs}(kD, 2, 1, 1)$ can be computed with standard numerical integration technique. Note that from symmetry, $F_{gs}(kD, 1, 2, 1) = F_{gs}(kD, 2, 1, 1)$.

Superposition can also be used to evaluate $F_{gg}(kD, 1, 1, 1)$ and $F_{gg}(kD, 1, 1, 2)$ (which is identical to $F_{gg}(kD, 1, 2, 1)$ and $F_{gg}(kD, 2, 1, 1)$ as defined by Eq. (7). These expressions are

$$F_{gg}(kD, 1, 1, 1) = 4 - \frac{1}{\pi}\int_0^1\int_0^1\int_0^1 P(kD, \eta_x, \eta_y, \eta_z)\,d\eta_x d\eta_y d\eta_z \qquad (A.11)$$

where

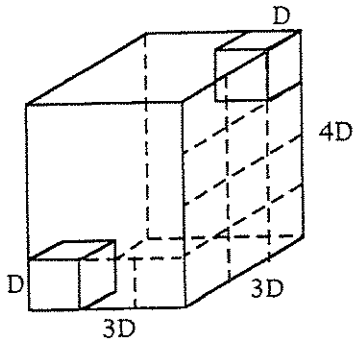

Figure A.1 Illustration of the numbering sequence convention for exchange factor $F_{gs}(kD, 3, 3, 4)$.

$$\begin{aligned} P(kD, \eta_x, \eta_y, \eta_z) = {} & N_1(kD, \eta_x, \eta_y, \eta_z) + N_1(kD, 1-\eta_x, \eta_y, \eta_z) \\ & + N_1(kD, \eta_y, \eta_x, \eta_z) + N_1(kD, 1-\eta_y, \eta_x, \eta_z) \\ & + N_1(kD, \eta_z, \eta_x, \eta_y) + N_1(kD, 1-\eta_z, \eta_x, \eta_y) \end{aligned} \qquad (A.12)$$

and

$$F_{gg}(kD, 1, 1, 2) = F_{gs}(kD, 1, 1, 1) - 4F_{gs}(kD, 2, 1, 1) - F_{gs}(kD, 1, 1, 2) \qquad (A.13)$$

where $F_{gs}(kD, 1, 1, 2)$ (for two disjoint elements) can be calculated by direct numerical integration.

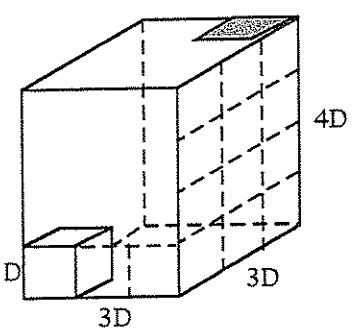

Figure A.2 Illustration of the numbering sequence convention for exchange factor $F_{gs}(kD, 3, 3, 4)$.

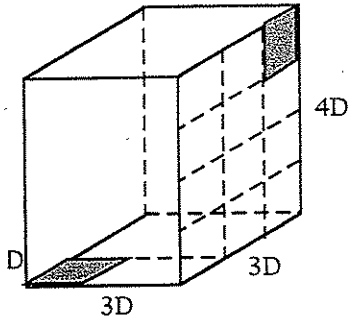

Figure A.3 Illustration of the numbering sequence convention for exchange factor $F_{ssi}(kD, 3, 3, 4)$.

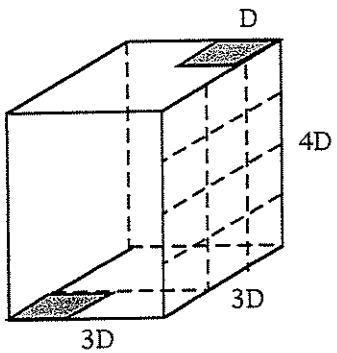

Figure A.4 Illustration of the numbering sequence convention for exchange factor $F_{ssp}(kD, 3, 3, 4)$.

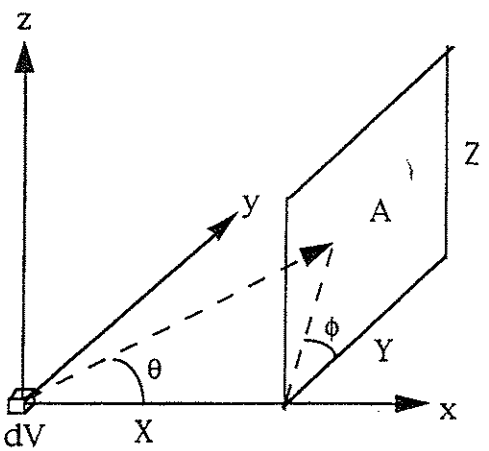

Figure A.5 Geometry and coordinate system used in the evaluation of Eq. A2.

APPENDIX B. DERIVATION OF THE AVERAGE REFLECTIVITY AND SCATTERING FACTOR FOR GZM

For the development of Eq. (53), consider a volume zone V_j and two area zones A_i, A_k as shown in Figure B.1. The net outgoing radiation from a differential volume dV_j, reflected by a differential area dA_i and intercepted by a differential area dA_k can be written as

$$d^3Q_{gj,i,k} = i'_{gj,i}(\vec{r}_j)\rho''(\vec{r}_i, \theta_{ji}, \phi_{ji}, \theta_{ki}, \phi_{ki})e^{-k(r_{ji}+r_{ki})} \frac{(\vec{r}_{ji}\cdot\vec{n}_i)(\vec{r}_{ki}\cdot\vec{n}_i)(\vec{r}_{ki}\cdot\vec{n}_k)}{r_{ji}^3\, r_{ki}^4} kdV_j dA_i dA_k \qquad (B.1)$$

In terms of the net outgoing radiosity $dW_{gj,i}$, the intensity $i'_{gj,i}$ can be written as

$$i'_{gj,i} = \frac{dW_{gj,i}}{\pi} \qquad (B.2)$$

Utilizing the definition of exchange of factor, Eq. (*B*.1) becomes

$$d^3Q_{gj,i,k} = \frac{\pi dW_{gj,i}}{dA_i}\rho''(\vec{r}_i, \theta_{ji}, \phi_{ji}, \theta_{ki}, \phi_{ki})(ds_i dg_j)(ds_i ds_k) \qquad (B.3)$$

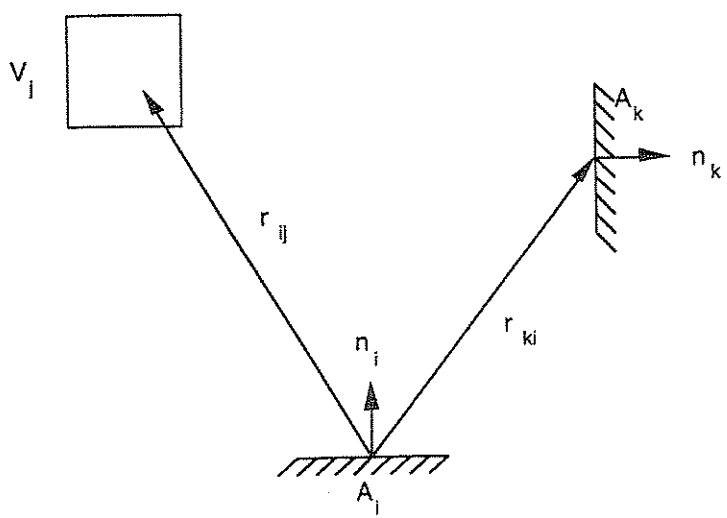

Figure B.1 Geometry and notation used in the development of Eq. 53.

In GZM, the radiosity from V_{gj} directed toward A_i is assumed to be constant. Integrating over V_{gj}, A_i, and A_k, Eq. (*B*.3) can be written as

$$Q_{gj,i,k} = \frac{\pi}{A_i} W_{gj,i}\left(s_i g_j\right)\left(s_i s_k\right)\hat{\rho}_{gj,i,k} \tag{B.4}$$

with $\hat{\rho}_{gj,i,k}$ given by Eq. (53).

Eq. (58) can be derived in a similar manner. Utilizing the geometry and notations as shown in Figure B.2, the net outgoing radiation from a differential volume dV_j, reflected by a differential volume dV_i and intercepted by a differential area dA_k can be written as

$$d^3Q_{gj,gi,k} = i'_{gj,gi}\left(\vec{r}_j\right)\omega\frac{\Phi\left(\cos\theta_{jik}\right)}{4\pi}e^{-k\left(r_{ji}+r_{ki}\right)}\frac{\left(\vec{r}_{ki}\cdot\vec{n}_k\right)}{r_{ji}^{\,2}r_{ki}^{\,3}}k^2dV_jdV_idA_k \tag{B.5}$$

In terms of the radiosity $dW_{gj,gi}$ and the various differential exchange factors, Eq. (*B*.5) becomes

$$d^3Q_{gj,gi,k} = \frac{\omega dW_{gj,gi}}{4kdV_i}\Phi\left(\cos\theta_{jik}\right)\left(dg_i dg_j\right)\left(dg_i ds_k\right) \tag{B.6}$$

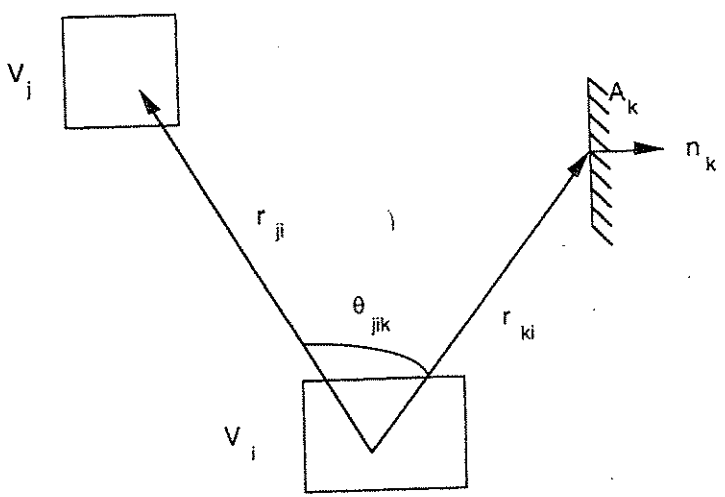

Figure B.2 Geometry and notation used in the development of Eq. 58.

Integrating over the finite volumes and area, Eq. (*B*.6) can be written as

$$Q_{gj,gi,k} = \frac{\omega}{4kV_i}W_{gj,gi}\left(g_i g_j\right)\left(g_i s_k\right)\hat{\Phi}_{gj,gi,k} \tag{B.7}$$

with $\hat{\Phi}_{gj,gi,k}$ given by Eq. (58).